NAVAL POSTGRADUATE SCHOOL
MONTEREY, CALIFORNIA

DTIC
S ELECTE
MAR 0 2 1994
B D
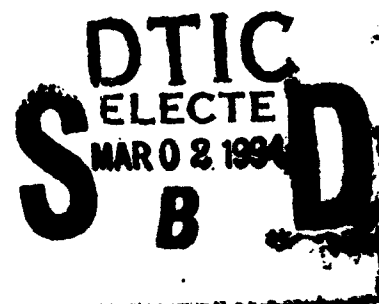
THESIS

Numerical Analysis of
Single-Vortex/Free-Surface Interaction

by

Craig F. Merrill

December 1993

Thesis Advisor: T. Sarpkaya

Approval for public release; distribution is unlimited.

94-06744

94 3 01 057

Best
Available
Copy

REPORT DOCUMENTATION PAGE		Form Approved OMB No. 0704-0188

1a. REPORT SECURITY CLASSIFICATION Unclassified	1b. RESTRICTIVE MARKINGS
2a. SECURITY CLASSIFICATION AUTHORITY	3. DISTRIBUTION AVAILABILITY OF REPORT
2b. DECLASSIFICATION/DOWNGRADING SCHEDULE	Approved for public release; distribution unlimited.
4. PERFORMING ORGANIZATION REPORT NUMBER(S)	5. MONITORING ORGANIZATION REPORT NUMBER(S)

6a. NAME OF PERFORMING ORGANIZATION Naval Postgraduate School	6B OFFICE SYMBOL (If applicable) ME	7a. NAME OF MONITORING ORGANIZATION Naval Postgraduate School
6c. Address (City, State, and ZIP Code) Monterey, CA 93943-5000		7b. ADDRESS (City, State, and ZIP Code) Monterey, CA 93943-5000
8a. NAME OF FUNDING/SPONSORING ORGANIZATION	8b OFFICE SYMBOL (If applicable)	9. PROCUREMENT INSTRUMENT IDENTIFICATION NUMBER
8c. ADDRESS (City, State, and ZIP Code)		10. SOURCE OF FUNDING NUMBERS

10. SOURCE OF FUNDING NUMBERS			
PROGRAM ELEMENT No.	PROJECT No.	TASK No.	WORK UNIT ACCESSION No.

11. TITLE (Include Security Classification) Numerical Analysis of Single-Vortex/Free-Surface Interaction

12. PERSONAL AUTHOR(S) CRAIG F. MERRILL

13a. TYPE OF REPORT Thesis for Master of Science and Mechanical Engineer Degrees	13b. TIME COVERED From:	14. DATE OF REPORT (Year, Month, Day) December 1993	15. PAGE COUNT 88

16. SUPPLEMENTARY NOTATION The views expressed in this thesis are those of the author and do not reflect the official policy or position of the Department of Defense or the U. S. Government.

17. COSATI CODES			18. SUBJECT TERMS (Continue on reverse if necessary and identify by block number) Surface Disturbances, Scars, Trailing Vortices, CFD
FIELD	GROUP	SUB-GROUP	

19. ABSTRACT (Continue on reverse if necessary and identify by block number)

The interaction of a single Lamb vortex with a free surface is analyzed numerically through the use of a finite-difference technique. The individual effects of gravity, viscosity, and surface tension are investigated within the range of the applicability of the phenomenon and the code used. The vortex is allowed to build up to its full strength in a relatively small time and then the evolution of the free surface, streamlines, and other details of the flow are calculated. The results have shown that the smaller the proximity of the vortex to the free surface, the larger the scar produced on its down-wash side. The effect of the surface tension is to reduce the amplitude of the free surface elevation. The viscous effects appear to be relatively small even though the calculations are, out of necessity, confined to a limited range of the governing parameters, as in all finite difference calculations.

20. DISTRIBUTION/AVAILABILITY OF ABSTRACT [X] UNCLASSIFIED/UNLIMITED [ ] SAME AS RPT. [ ] DTIC USERS	21. ABSTRACT SECURITY CLASSIFICATION Unclassified	
22a. NAME OF RESPONSIBLE INDIVIDUAL Professor T. Sarpkaya	22b TELEPHONE (Include Area code) (408) 656-3425	22c. OFFICE SYMBOL ME-SL

i

Numerical Analysis of
Single-Vortex/Free-Surface Interaction

by

Craig F. Merrill
Lieutenant, United States Navy
B.S. United States Naval Academy, 1986

Submitted in partial fulfillment of the
requirements for the degree of

MASTER OF SCIENCE IN MECHANICAL ENGINEERING

AND

MECHANICAL ENGINEER

from the

NAVAL POSTGRADUATE SCHOOL

December 1993

Author: _____
Craig F. Merrill

Approved by: _____
T. Sarpkaya, Thesis Advisor

_____
Matthew D. Kelleher, Chairman,
Department of Mechanical Engineering

_____
Richard S. Elster, Dean of Instruction

ii

ABSTRACT

The interaction of a single Lamb vortex with a free surface is analyzed numerically through the use of a finite-difference technique. The individual effects of gravity, viscosity, and surface tension are investigated within the range of the applicability of the phenomenon and the code used. The vortex is allowed to build up to its full strength in a relatively small time and then the evolution of the free surface, streamlines, and other details of the flow are calculated. The results have shown that the smaller the proximity of the vortex to the free surface, the larger the scar produced on its down-wash side. The effect of the surface tension is to reduce the amplitude of the free surface elevation. The viscous effects appear to be relatively small even though the calculations are, out of necessity, confined to a limited range of the governing parameters, as in all finite difference calculations.

iii

TABLE OF CONTENTS

LIST OF TABLES

LIST OF FIGURES

LIST OF SYMBOLS

α Non-dimensional vortex core radius, r_0/h_0

Fr   Froude number, $\Gamma/\left(h_0\sqrt{gh_0}\right)$

g   Gravitational acceleration

h_0 Depth of vortex below free surface

Re   Reynolds number, $h_0\sqrt{gh_0}/\upsilon$

r_0 Vortex core radius

t   Time, seconds

T   Non-dimensional time, $t\sqrt{g/h_0}$

v   Transverse component of velocity

V   Total vortex induced velocity

V_{MAX} Total vortex induced velocity at r_0

w   Vertical component of velocity

We   Weber number, $\sigma/\left(\rho gh_0^2\right)$

y   Transverse coordinate

y_c Transverse position of center of vortex core

z   Vertical coordinate

z_c Vertical position of center of vortex core

Γ Circulation of vortex

ρ Fluid density

σ Surface tension

ν Kinematic viscosity

ACKNOWLEDGMENTS

I. INTRODUCTION

The study of the flow about a submerged foil, in general, and a foil in the vicinity of a free surface, in particular, has a number of applications in hydrodynamics. For example, the effect of the free surface on the performance characteristics of partially submerged bodies, the stability of flow about control surfaces, and the surface signature created by the wake of a foil have emerged as important problems during the past decade. In these applications, the effects of gravity, viscosity and surface tension are almost equally important. The gravitational forces control the shape and the amplitude of the surface disturbances, viscous forces control in a more subtle manner the curvature of the surface and the rate of decay of the flow structures, and the surface tension controls the magnitude of the gradients and strains at the surface, and, thereby, the amplitude of the disturbances, together with the gravitational forces. It is, therefore, of paramount importance that all numerical calculations attempting to predict the behavior of flow resulting from a submerged or partially submerged foil account for all three effects in a three dimensional flow and, if not yet possible, in a relatively more manageable two-dimensional flow situation.

As far as the recent naval hydrodynamic applications are concerned, the emergence of the remote control and observation technology, combined with the emergence of surface signatures, precipitated by the motion of near-surface submerged bodies, gave rise to the explorations of the non-acoustic detection of submerged bodies. Even though the technology is rather new

1

and the exploration of its potential requires the understanding of many satellite technologies, the preliminary investigations have shown its potential and forged many interesting studies in the past few years.

The first such investigation was undertaken by Sarpkaya and Henderson (1984) who have shown that the interaction of an ascending vortex pair with a free surface gives rise to scars and striations. The scars are relatively deep and long depressions on the downwash side of each vortex and are comprised of many vortices with axes normal to the free surface. These scars are bridged by the so-called striations which give the appearance of the rungs of a ladder. The character of these scars and striations are such that they give rise to coherent structures whose scale and frequency band are in the range of those of the Brag frequency. Thus, the alteration of the scale of the near-surface coherent structures (e.g., vortices or whirls) by single or double trailing vortices serves as a Brag-frequency discriminator and provides the connection between the non-acoustic detection of submerged bodies and the study of surface signatures.

The realization of the foregoing led to considerable work in recent years on the interaction of vortices, wakes, and other types of flow with deformable fluid interfaces, all characterizable by the more general phenomenon of the interaction of vorticity with rigid and stratified deformable boundaries. Experimental work has ranged from the study of the interaction of submerged jets with a free surface, to the study of the interfacial turbulence in grid-stirred tanks. Numerical investigations have ranged from the use of vortex dynamics for inviscid flows to the use of finite-difference techniques for the

solution of two-dimensional viscous and incompressible flows (with or without linearization at the free surface).

The interaction of an ascending vortex pair with a free surface was analyzed in detail by Ohring and Lugt (1991) through the use of the full Navier-Stokes equations for an incompressible two-dimensional viscous flow, including surface tension and surface-generated vorticity. Out of necessity, their calculations were confined to relatively small Reynolds numbers (suitably defined in terms of the velocity of the ascending vortices , the initial vortex spacing and the fluid viscosity) in order to maintain stability and convergence. The effects of the Froude number (representing gravity) and those of the Weber number (representing surface tension) were properly accounted for. It is of importance to note that the value of the Reynolds number is not of particular concern for their investigation since their objectives were not so much the simulation of the ocean-truth or of the establishment of a practical predictive model, but rather the understanding of the physics of the phenomenon as to the size and evolution of the scars and the effect of the secondary vorticity on the motion of the primary vortices. The inclusion of the effects of surface tension were to shed further light on the anticipated effects of surface contamination which invariably exists in the oceans.

Ohring and Lugt have shown that:

High and low Froude numbers represent the two extremes of free surface yielding and stiffness, respectively. For an intermediate Froude number, a special rebounding due to the presence of secondary vortices has been observed: the path of the primary vortex centre portrays a complete loop (Ohring and Lugt, 1991, p.47).

3

They have also shown that for relatively high Froude numbers (i.e., larger deformations) and for Reynolds numbers larger than about 50, the predictions do not appear to be strongly dependent on the Reynolds number, within the range of Reynolds numbers considered by them. In other words, the free-surface deformation without the influence of the surface tension is determined strongly by the gravitational effects or the Froude number. When the surface tension effects are included, the larger the Weber number, the larger the attenuation of the surface elevation, as shown by Ohring and Lugt (1991). This, however, raises the important question that the delineation of the effect of the Reynolds number on the results might depend not only on the magnitude of the Froude number but also on the Weber number since their increasing values produce opposing effects of the surface elevation. Thus, if the large Froude numbers give rise to larger elevation and thereby lessen the effect of the Reynolds number and the larger Weber numbers reduce the surface elevation and tend to intensify the importance of Reynolds number, it would be rather difficult to ascertain their respective roles when both the viscous and surface tension effects are included. Nevertheless, the choices for the numerical analysist dealing with the Navier-Stokes equations are limited partly by the stability and convergence of the solutions and partly, and perhaps more importantly, by the stability of the phenomenon itself.

As far as the effect of a single vortex on the free surface is concerned, only Tyvand (1991) considered a vortex placed suddenly near a free surface and attempted to calculate the resulting wave phenomena for an inviscid case. His calculations, valid only for very short times, have shown that the sudden introduction of the vortex does not give rise to waves. This fact has

already been established by others. Tyvand (1991) did not show any longtime calculations, streamlines, or surface deformations.

The present investigation is a detailed solution of the two-dimensional Navier-Stokes equations for a viscous, incompressible fluid with a viscous vortex placed below the free surface. The finite-difference code used in the calculations will be described in the following sections.

II. NUMERICAL REPRESENTATION

A INTRODUCTION TO PROGRAM

The numerical analysis discussed herein was performed using the RIPPLE computer program which was specifically designed to model "transient, two-dimensional, incompressible fluid flows with surface tension on free surfaces of general topology" (Kothe, Mjolsness, and Torrey, 1991). The code was modified to the extent necessary to solve the vortex/free-surface interaction problem and to produce the numerical and graphical results. All of the subroutines required for performing the numerical solution were organic to the program.

RIPPLE solves either the Euler or the Navier-Stokes equations for incompressible fluids (with or without surface tension), using a two-step projection finite difference scheme which is second-order accurate in space and first-order accurate in time. It is capable of solving in either a Cartesian or cylindrical two-dimensional coordinate system, using a uniform or varied mesh, and, has the ability to model curved boundaries and internal obstacles using various types of boundary conditions.

B. DESCRIPTION OF PROGRAM

The following brief description of the numerical method follows closely that given by Kothe, Mjolsness, and Torrey (1991).

The governing equations are the continuity equation for an incompressible fluid,

$$\nabla \bullet \overline{V} = 0 \tag{1}$$

and the momentum equations,

$$\frac{\partial \overline{V}}{\partial t} + \nabla \bullet \left(\overline{VV} \right) = -\frac{1}{\rho} \nabla p + \frac{1}{\rho} \nabla \bullet \tau + \overline{g} + \frac{1}{\rho} \overline{F}_b \tag{2}$$

where τ, is the viscous stress tensor for a Newtonian fluid, ρ the fluid density, p the pressure, g the acceleration due to gravity and F_b the total body force. The particular properties of the fluid are assigned positions within a given computational cell as shown in Figure 1.
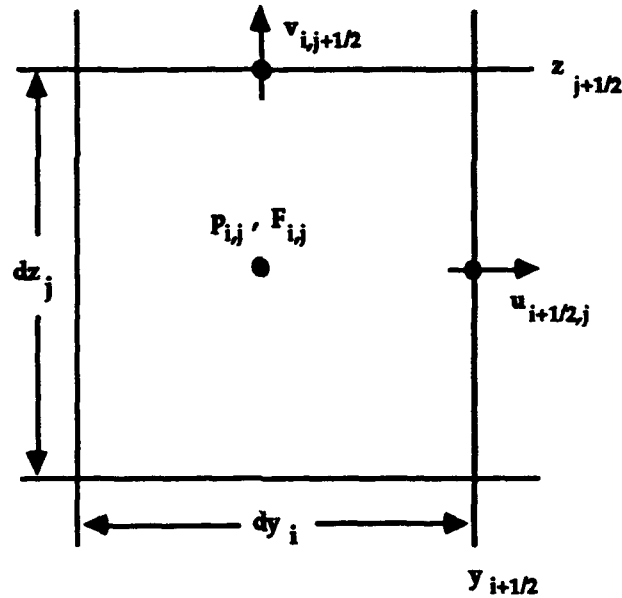

Figure. 1 Cell Definition in the Grid (Kothe, Mjolsness, and Torrey, 1991)

For the two-step projection method, Equation (2) is discritized with respect to time as,

7

$$\frac{\overline{V}^{n+1} - \overline{V}^n}{\delta t} = -\nabla \bullet \left(\overline{VV}\right)^n - \frac{1}{\rho^n}\nabla p^{n+1} + \frac{1}{\rho^n}\nabla \bullet \tau^n + \overline{g}^n + \frac{1}{\rho^n}\overline{F}_b^n \qquad (3)$$

The only implicit term in this equation is pressure—all others terms are approximated according to their values at the previous time step. The first step of the projection scheme solves for a velocity field based on incremental changes in the explicit terms of Equation (3). The second combines this intermediate velocity field and the pressure term of Equation (3) with Equation (1) to calculate the velocity field at the next time step. This combination forms a Poisson's equation which is solved using an incomplete Cholesky conjugate gradient (ICCG) matrix solver. The momentum advection term of Equation (3) is solved using the second-order upwind method of van Leer.

When solving for the free surface, the program assumes that the surface tension, σ, is constant and that the viscous stresses at the free surface may be neglected. This allows for the application of the continuum surface force (CSF) which represents the surface tension as an equivalent volume force rather than a pressure jump (Brackbill, Kothe, and Zemach, 1992). Thus, the free surface discontinuity is replaced with a smooth transition, or "color," which varies across any computational mesh cell containing a free surface. The volume force is non zero only within these cells and is solved as one component of the body force term in Equation (3). A contact angle, θ, may be defined at any boundary and used to approximate wall adhesion forces. Because surface tension is solved explicitly, it is subjected to a linear stability time step constraint.

Numerous techniques have been developed to perform the non-trivial task of modeling the free surface of a fluid. The method employed in RIPPLE is the Volume-of-Fluid (VOF) method. VOF is a donor-acceptor differencing technique which makes use of a scalar field function, F, to act as a marker of the free surface. F describes the fraction of a cell which is occupied by the fluid:

$$F(x,t) = 1 \quad \text{in the fluid;}$$
$$F(x,t) = 0 \quad \text{in the void; and,}$$
$$0 < F(x,t) < 1 \quad \text{at the free surface.}$$

The free surface, therefore, is not continuous, but rather, is represented by a series of discontinuous line segments described by the value F in the surface cells. Although, a reconstructed free surface is not required for surface tension calculations (since this is handled by the CSF model), it is needed to ensure that the fluid in the vicinity of the free surface is accurately advected over the domain. Both the reconstruction and advection of the VOF function is performed using a Hirt-Nichols (H-N) algorithm. Because the H-N algorithm is explicit in time, the maximum time step is subject to the Courant condition. Also, the fluid color, used in the CSF model is related to the VOF function. The viscous stress term is solved explicitly in time using a backward difference scheme, so it too is subjected to a linear stability time step constraint.

9

C. PROGRAM PARAMETERS

The first parameter which must be chosen is the size of the domain. Because it is desirable to limit the problem run-time to some reasonable length, excessively large domains are impractical. Therefore, the size of the domain must be limited, while simultaneously minimizing the impact of the resulting boundaries which must be in relatively close proximity to the region of concern. Given an initial vortex depth below the free surface of h_0, it was found to be sufficient to place the side boundaries at $\pm 4h_0$ and the lower boundary at $3h_0$, below the vortex center, for a Froude number Fr (= $\Gamma/h_0\sqrt{gh_0}$) = 7.5. For Fr = 13.8, the side boundaries were placed at $\pm 6h_0$ and the lower boundary at $5h_0$. The top boundary needed to be located high enough above the free surface so as not to interfere with the largest vortex-induced free-surface deformation. For this analysis, $1.7h_0$ was deemed sufficient.

Closely related to the size of the domain is the type of boundary conditions imposed on its periphery. RIPPLE is capable of applying free-slip, no-slip, periodic, applied pressure, continuative outflow or a specified inflow/outflow condition to any of the four boundaries. The last three conditions have no relation to this problem. The no-slip condition is not appropriate because it enhances the influence the boundaries have upon the domain. The periodic condition simply reflects the velocities, pressures and free surface positions about the boundary and does not accurately represent the images produced by a single vortex. The free-slip condition is ultimately the best choice since it limits the effect of the boundaries and crudely models the vortex images on the sides and bottom of the domain.

10

The grid size can be either uniform or varied in either direction. Because a varied grid is applied along the entire length of the domain (for example, a variation in the grid in the y-direction must be applied from the bottom to the top of the domain) the number of cells are increased along the entire strip and not just in the region desired. It is as a consequence of the decrease of the cell size in such regions that the demand for CPU time increases. Thus, a choice must be made between the increase of the CPU time and the increase of the accuracy of the computation over a "cross-shaped" refined region. A uniform mesh was, therefore, used with its coarseness limited by RIPPLE's ability to accurately solve for the free surface for the given values of the Froude number ($Fr = \Gamma/h_0\sqrt{gh_0}$), the Weber number ($We = \sigma/\rho gh_0^2$), and the Reynolds number ($Re = h_0\sqrt{gh_0}/\nu$). A 192x112 mesh grid was capable of meeting the needs of this analysis within a reasonable run-time using a SUN SPARCstation 10™ (25 to 70 hours).

The program provides for a choice between a fixed time step and a variable time step (adjusted automatically during the course of the calculation). Regardless of which method is chosen, the code requires that an initial time step and a maximum allowed time step be provided. For this analysis, the variable time step was used because it reduced the run-time while making sure that the linear stability requirements were met. It was also determined that an initial time step approximately equal to 1/10-th of the maximum time step of the three time constraints was sufficient. For initial time steps larger than that, the code frequently exceeded one of the time constraints, requiring it to recalculate the current time step.

11

As was the case for the grid size, the tradeoff for defining the required convergence criteria for the Poisson pressure solver was the solution-accuracy versus problem run-time. Through limited trial-and-error, it was found that a value of 0.001 was acceptable.

As described previously, the advection calculation is performed explicitly with respect to time and must, therefore, meet the Courant criteria. Implicit in the program is the assumption that all time steps have Courant numbers less than 0.5 — any step not meeting this criteria must be recalculated. To prevent an inordinate amount of recalculation, the Courant number was set to 0.38. This ensured that the Courant number after the calculation was less than 0.5 and that the advection solution remained stable. The program also allows for choosing the type of momentum advection. Based on the recommendation of the authors, van Leer's method was used.

D. ADDITIONAL PARAMETERS

A code such as RIPPLE allows the user to define numerous parameters and variables, but it obviously cannot anticipate every particular situation to be encountered. The interaction of the vortex with the free surface had to be correctly implemented and incorporated into the code, together with the selection of the appropriate boundary conditions and parameters which are compatible with the demands of the flow field. Therefore, it was necessary to include a routine which defined the desired vortex and the variables necessary to vary the governing parameters associated with the simulation (Fr, We, Re and $\alpha = r_0/h_0$, the ratio of the core size to the depth of the vortex).

A subroutine designed to specify the boundary conditions was modified to characterize a single vortex. The swirling motion was prescribed over a square region, surrounding the vortex core. The velocities were solved using the velocity equation derived from the Lamb vortex model in Cartesian coordinates,

$$V(y,z,t) = \frac{\Gamma(t)}{2\pi\sqrt{y^2+z^2}}\left[1-\exp\left\{-1.2544\left(\frac{y^2+z^2}{r_0^2}\right)\right\}\right]$$ (4)

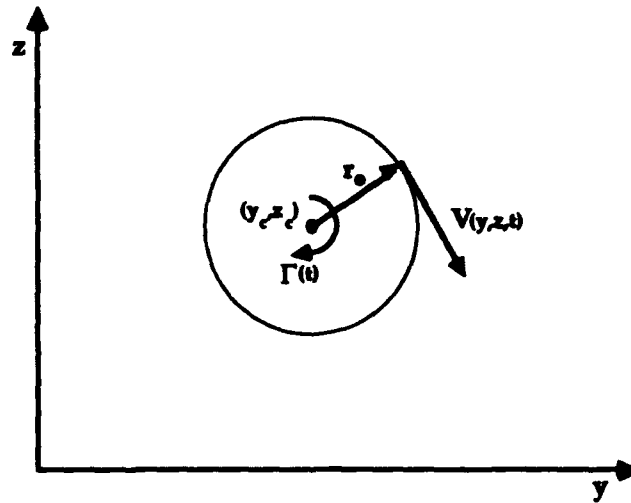where Γ is the vortex strength, r_0 the vortex core radius and y and z as shown in Figure (2).

Figure. 2 Definition of Vortex Characteristics

The v and w components of velocity are then given by,

$$v(y,z,t) = V(y,z,t)\left[\frac{z}{\sqrt{y^2+z^2}}\right]$$ (5)

and

$$w(y,z,t) = -V(y,z,t)\left[\frac{y}{\sqrt{y^2 + z^2}}\right] \quad (6)$$

This required the ability to define Γ, r_0 and the location of the vortex center, (y_c, z_c). The length of the sides of the square region in which these velocities were defined was set equal to $3r_0$, with $1/3 \leq \alpha \leq 1/2$.

It was recognized that to place the vortex instantly at full strength at time $T (= h_0/\sqrt{g}) = 0$ would likely "shock" the system, thereby requiring long run-times to allow an equilibrium condition to establish at the free surface. Thus, the vortex was initialized at some fraction of its ultimate strength, and allowed to build up linearly over a predetermined time period. Typically, the vortex was initialized at 0.01Γ and allowed $7T$ to $10T$ normalized times, to reach full strength. It was desired that the vortex/free-surface interaction be examined in a "natural state," where not only was the free surface shaped by the vortex, but the vortex distorted and moved by the free surface. It was, therefore, necessary to cease providing the vortex with a source of circulation so that both the vortex and the surrounding flow field could reach a non-forced state of relaxation. Subsequently, the quasi-steady state of the interaction was examined. To achieve this, one last parameter was added which specified the time at which the velocities within the square region surrounding the core would no longer be redefined. For all of this analysis, this time occurred at $25T$, as this was sufficient to allow the free surface to reach a state of dynamic equilibrium, yet early enough to prevent the

14

boundaries from influencing the interaction. After reviewing the graphical output from numerous runs, it was determined that the best time at which to examine and compare the above interaction was 27T. Most of the runs were continued far beyond the time 27T. An example of the evolution and demise of a single vortex at larger times is presented in the discussion of results.

III. PRESENTATION AND DISCUSSION OF RESULTS

A. INTRODUCTION

Among the numerous calculations performed, only six representative single-vortex/free-surface interactions will be discussed in some detail. The six runs are classified according to the combination of the Froude, Reynolds, and Weber numbers:

TABLE 1: THE RANGE OF THE GOVERNING PARAMETERS

Set #1	Fr = 7.50	Re = 40	We = 0.033
Set #2	Fr = 7.50	Re = 20	We = 0.033
Set #3	Fr = 7.50	Re = 40	We = 0.333
Set #4	Fr = 7.50	Re = 20	We = 0.333
Set #5	Fr = 13.80	Re = 40	We = 0.333
Set #6	Fr = 13.80	Re = 20	We = 0.333

Each set of calculations show the streamlines, velocity vector plots, v/V_{MAX} versus y/h_0, w/V_{MAX} versus y/h_0, v/V_{MAX} versus z/h_0, and w/V_{MAX} versus z/h_0.

B. ASSESSMENT OF THE EFFECTS OF VISCOSITY

As noted from the foregoing table, the first two sets of runs are designed to evaluate the effect of the Reynolds number, however small the range of the Reynolds number may be. The comparison of Figures 3 and 9, 4 and 10, 5

16

and 11, and 6 and 12 show that aside from the secondary details in the vicinity of the vortex core, the shape and magnitude of the free-surface deformation are nearly identical. The secondary differences, attributable to the rate of diffusion, show in the straining of the vortex, in the vorticity contours around the primary vortex, and in the shape of the streamlines surrounding the primary core. It is noted that for the case of the smaller Reynolds number (Figure 9), the lower part of the main vortex is comprised of two cells of streamlines whereas the one for Re = 40 (Figure 3) is less diffused and the streamlines below extend over larger regions. In other words, there are subtle differences between the two streamlines in spite of the relatively small difference between the two Reynolds numbers. It will be shown later that the said differences are further enhanced with increasing Froude number and decreasing Weber number.

Figures 5 and 11 show the v-component of the normalized velocity on a transverse line passing half-way between the original positions of the free surface and the vortex center ($z/h_0 = 0.50$). The magnitude and direction of this velocity along the y-axis depends on the particular position of the z = constant plane. For a non-deformaing free surface, it can be demonstrated through the use of a Kelvin oval that the velocity should be maximum directly above the vortex and decrease symmetrically as the distance from the vortex increases as shown in the insets of Figures 5 and 11. The reasons for the change of direction as well as the difference in the magnitudes of the negative values of the v-component are a consequence of the asymmetric deformation of the free surface on either side of the z-axis. The rise in water elevation and the drop in the v-velocity to negative values on the upwash

17

side of the vortex are both larger for reasons which can be easily explained by examining the streamlines and the velocity vector plots.

The w/V_{MAX} versus y/h_0 is shown in Figures 6 and 12 for the governing parameters of the first two sets of calculations, shown in Table 1. In these plots several facts are evident: (i) the velocity profile is not odd-symmetric with respect to the z-axis, as it would have been had the free surface remained undeformed; (ii) the magnitudes of the regions to the left and the right of the z-axis are significantly different, again due to the asymmetric deformation of the free surface; (iii) for the smaller Reynolds number case (Figure 12), the w profile is relatively more symmetric, as would be expected; and (iv) in both cases, w approaches zero from negative values on the left and from positive values on the right.

The transverse component of the velocity, v/V_{MAX}, versus z/h_0 is shown in Figures 7 and 13 for the two calculations under consideration. Aside from their magnitudes, the two profiles are virtually identical. It is noted that the vortex center has shifted slightly downward in time due to the mutual interaction. It is also noted that the velocity profile is not symmetric with respect to the $z = 0$ line because of the proximity of the free-surface. Furthermore, the ratio of the velocity extrema is larger than unit for the larger Reynolds number case whereas it is smaller than unity for the lower Re case.

Finally, the variation of w/V_{MAX} with z/h_0 is shown in Figures 8 and 14. Normally, this velocity should be zero for a non-deforming surface. Thus, however small, the magnitude of w/V_{MAX} is one of the most important measures of the deformation of the free surface, i.e., the larger and more

asymmetric the deformation is, the larger the deviation of the w-component of velocity from zero. Figures 8 and 14 show that for a vortex rotating clockwise below the free surface, w becomes plus below the vortex axis and negative above the axis. In other words, there is mass flux into the vortex core in the z-direction. It can be shown, however, that the net mass flux into the core around a circumference is zero by virtue of the solenoidality of the flow.

C. ASSESSMENT OF THE EFFECTS OF SURFACE TENSION

Now, the calculation sets of 3 and 4 (see Table 1) will be discussed. It should be noted that these two sets differ from the first two only in terms of the Weber number. Thus, the sets 1 and 3 and sets 2 and 4 have identical Froude and Reynolds number and any differences in their characteristics will be indicative of the increase in the surface tension or of the Weber number. In assessing the role of the Weber number on the flow behavior, it should also be noted that the surface tension has been increased by ten fold whereas the Reynolds number was only doubled.

Figures 15 and 21 show the streamlines for cases 3 and 4. The first striking difference between the two figures is the magnitude of the deformation of the free surface: the smaller the Weber number, the larger is the deformation. This is somewhat expected on the grounds that the additional surface tension gives rise to surface tension gradients and surface vorticity and these in turn absorb energy which would have been otherwise stored in the fluid as potential energy in raising the free surface. A similar conclusion can be drawn regarding the low Reynolds number case, as seen in

Figures 9 and 21. A closer examination of the streamlines very near the region where the free-surface slope changes (nearly above the vortex) show that for small Reynolds numbers ($Re = 20$), the build-up of surface vorticity is somewhat stronger than the higher Reynolds number cases. This is expected on the grounds that the flatness of the surface and the diffusion of vorticity in the lateral directions should lead to secondary circulations between the vortex and the free surface.

The vector plots of the velocity are shown in Figures 4 ($Fr = 7.50$, $Re = 40$, $We = 0.033$) and 16 ($Fr = 7.50$, $Re = 40$, $We = 0.333$) and in Figures 10 ($Fr = 7.50$, $Re = 20$, $We = 0.033$) and 22 ($Fr = 7.50$, $Re = 20$, $We = 0.333$). These figures show that even though such vector plots are valuable in pointing out the direction and magnitude of the velocities, they do not allow one to develop an integrated mental image to draw conclusions regarding the interaction between the vortex and the free surface. These can only be achieved through a careful perusal of the velocity distributions along selected lines and directions.

The second most significant impact of the surface tension must surely be associated with and be a consequence of the flattening of the free surface. Namely, the velocities in the transverse direction are enhanced as the streamlines are confined to narrower regions above the vortex (e.g., at $z/h_o = 0.5$, as in the present case) and the v/V_{MAX} values should be larger for the case of $We = 0.333$ than for $We = 0.033$, as seen in Figures 17 and 5, respectively. Figures 11 and 23 exhibit the same behavior, but less dramatically.

The vertical component of velocity along a transverse plane ($z/h_o = 0.50$) for the case of $Fr = 7.50$, $Re = 40$, and $We = 0.333$ (Figure 18) may now be

compared with that for Fr = 7.50, Re = 40, and We = 0.033 (Figure 6). Apparently, due to the elevation of the transverse plane the difference in w is not as accentuated as the v-component. In fact, the solenoidality of the flow for a given vortex position necessitates that the increased v-velocities (the bunching of the streamlines) should be compensated for by a smaller difference in the w component. For the case of the lower Reynolds number, Figures 12 (Fr = 7.50, Re = 20, and We = 0.033) and 24 (Fr = 7.50, Re = 20, and We = 0.333) support the same conclusion.

A comparison of Figures 18 through 20 for (Fr = 7.50, Re = 40, and We = 0.333) with Figures 24 through 26 for (Fr = 7.50, Re = 20, and We = 0.333) shows that the dependence on the Reynolds number of the particular velocities are not significant and certainly no more than that described earlier. It suffices to note that the most important difference is in the v-component of the velocity and the degree of the differences on all velocities, including v, depend strongly on the proximity of the transverse plane to the deformed free surface. Here, it is implied that the difference is only in the magnitude of the velocities and not in the physics of the phenomenon. In other words, no new physical events are expected to occur as one approaches the free surface. It is also important to be reminded of the fact that these calculations deal only with laminar flows. In turbulent flows, the interaction of vorticity with the free surface gives rise to coherent flow structures which cannot be predicted here through laminar flow solutions (Sarpkaya and Suthon, 1991). Nevertheless, the overall behavior of the free surface, the generation of free-surface vorticity, mean-flow characteristics, the regions of formation of the primary and secondary vortices, the relative influence of various parameters

21

and several other experiment-guiding results can be predicted through the use of laminar flow calculations. It is on the basis of such results that turbulent flow measurements can be made to delineate the character of coherent structures and the transfer of vorticity from the vortex to the free surface and the generation of new structures and their redistribution in the transverse plane in the form of quasi-coherent quanta.

D. ASSESSMENT OF THE EFFECTS GRAVITY

The next issue to be taken up is the effect of the Froude number on the characteristics of the flow. The calculations are presented in sets 5 and 6 (see Table 1). The role played by the Froude number (signifying the effects of gravity) will be illustrated through the comparison of the results between the sets 3 (Fr = 7.50, Re = 40, We = 0.333) and 5 (Fr = 13.80, Re = 40, We = 0.333), and sets 4 (Fr = 7.50, Re = 20, We = 0.333) and 6 (Fr = 13.80, Re = 20, We = 0.333).

Figures 27 and 15 show that there are two fundamental differences between them. First, the surface elevation is larger for the larger Froude number. Second, the secondary vorticity is much more pronounced. Both of these effects are somewhat intuitive and could have been predicted in gross terms. However, the exact shape of the free surface, the deformation of the vortex and the relatively larger excursion of the vortex center seen with the larger Froude number could not have been anticipated. Figures 27 and 28 show that the vortex center, which was at (0, 0) at time zero, has gradually shifted to the third quadrant of the coordinate axis, but near the origin. Additional comments may be made regarding the streamlines and the

vorticity distribution in the regions below the vortex. Even though they further show the effects of the magnitude of the Froude number, here the attention will be concentrated on the near surface structures.

Figures 29 and 17 show that differences between the two Froude numbers is accentuated. Likewise, Figures 30 and 18 show that the overall character of the variation of the w-component is quite similar for the two Froude number cases, except for the fact the growth of the larger secondary vorticity, particularly to the right of the scar, gives rise to a 'hump' in the w-velocity as shown in Figure 30. This is expected to be further amplified in the transverse planes closer to the free surface. Figures 31 and 19 show that the v-component of the velocity is dramatically effected by the magnitude of deformation of the free surface as exemplified by the strong asymmetry of the top and bottom halves of the profile and by the absolute values of its magnitude. Finally, the w-component of velocity along the z axis is compared in Figures 32 and 20. As noted earlier, this velocity component is rather small for obvious reasons. Thus, its distribution is strongly influenced by any parameter, large or small. In this case, the migration of the center of the vortex, induced by the proximity and the degree of deformation of the free surface, could and has changed the distribution of the w-component. The vortex center in Figure 32 is such that this velocity component is negative through the entire z-axis, unlike the previous ones. The unidirectionality of the w-component along a single z-axis does not change the fact the mass flux through the vortex is maintained.

It is clear from the foregoing that the Reynolds number effects are subtle and the degree of diffusion of vorticity exhibits itself in all velocity profiles.

The effect of the Froude number is to amplify the magnitude of the deformations, enhance the secondary vorticity generation indirectly through the increase of the radius of curvature of the free surface, and through the straining of the vortex. The effect of the Weber number, however, is opposite to its magnitude in practically all aspects of the evolution of the flow. The larger the Weber number, the smaller are the deformations. In that sense, the surface tension and gravity effects act in opposite directions. Thus, one would expect that the cases of relatively low Froude and Weber numbers (e.g., Figures 3-8) and the cases of relatively high Froude number and Weber number (e.g., Figures 27-32) should be comparable. In fact Figures 3 and 27 show that the free surface deformations are comparable. They also show that the near doubling of the Froude number has a greater influence on the magnitude of the free surface deformation then the ten fold increase of the Weber number.

E. GROWTH AND DECAY OF THE VORTEX

In the foregoing, the effects of viscosity, surface tension, and gravity on the interaction of a vortex with a deformable free surface have been discussed at a specific time without regard to the transient state. These have been instructive in clarifying the combined as well as separate effects of the fundamental physical parameters and in paving the path to the design of physical experiments. Clearly, it would be equally important to know as to how a particular state has been reached and how the vortex decays with time if its circulation were no longer maintained constant. This section deals with these issues.

In view of the fact that it will be nearly impossible to discuss the evolution of a fluid state for all possible combinations of the governing parameters, only the most representative values of the Froude, Reynolds, and Weber numbers were chosen, i.e., Fr = 7.50, Re = 40, We = 0.033 (case 1).

Figures 39 through 47 show, starting at T = 10, the evolution of the streamlines. At time T = 10, the vortex has already reached its full strength. The circulation is held constant between the times T = 7 to T = 25. For T > 25, the vorticity of the vortex is allowed to diffuse without the infusion of new vorticity into the core. Thus, the circulation in the original core is allowed to decrease with time.

A cursory examination of the figures 39 through 43 (at T = 26) shows that the free surface quickly reaches its steady state shortly after T = 10. However, after T ≥ 26 (Figure 43), the diffusion of the unreplenished vortex begins to manifest its effects on the entire flow in the form of decreasing surface elevation, uniformalizing of the streamlines (showing that the vorticity gradients are becoming less steep), and the scar becoming more smooth. The surprising aspect of the decay process is that a steady state which has been essentially arrived at by T = 10 is largely maintained even at times as large as T = 30, at least in the immediate vicinity of the vortex. This is an indication of the longevity of the larger structures near the surface. The measurements previously carried out at Naval Postgraduate School (see, e.g., Neubert 1992) show that energy can cascade towards larger structures and thereby decay at a slower rate. That decay is certainly a function of a number of factors. Aside from the domain in which the vortex is born and subjected to decay, the condition of the free surface at a particular instant, the viscous, gravitational,

and the surface tension effects (surface contamination) will certainly influence the duration of the life of the vortex. If one were to assess the half-life of the vortex in terms of its decay to half the vortex strength, one might conjecture that this would be a very large time, not assessed in the present investigation due to CPU limitations.

IV. CONCLUSIONS

The interaction of a single Lamb vortex with a free surface has been modeled using a finite-difference scheme. The values of the Reynolds, Weber and Froude numbers were varied and the results compared in an effort to assertain the influence of viscosity, surface tension and gravity upon this interaction.

Compared to that of surface tension and gravity, the influence of viscosity on the evolution and steady-state of the surface deformation is rather secondary. Its major contribution is that of controlling the rate of diffusion and degree of vortex strain.

Within the range of Reynolds numbers examined, the effect of surface tension is to moderate the effect of the remaining parameters upon the interaction. In most cases, the result of an increase in the value of the surface tension, or Weber number, is opposite to that of the Froude number.

The gravitational force has the most notable influence on the vortex/free-surface interaction since it changes the curvature of the free surface with increasing circulation or with decreasing proximity to the free surface. Furthermore, the gravitational force indirectly controls the amount of vorticity generated at the free surface.

All of the foregoing is influenced to varying degrees of intensity, as well as complexity, by the non-symmetric nature of the free surface. This leads, among other things, to the stretching and tilting of the vortex, the flow of surface vorticity to the downwash side of the vortex, and, most importantly,

to the distributions of the v and w-components of the velocity. The v-component increases with the decrease of the vortex depth and with the flattening of the free surface. The w-component may be both positive or positive-negative depending on the elevation of the vertical line along which the velocity is calculated, the time of the calculation, and on the magnitude of the governing parameters.

The results have demonstrated that the deformation of the free surface for two-dimensional laminar states can be calculated through the use of a finite-difference code, capable of including all three effects: viscosity, surface tension and gravity.

It remains to be seen as to what the effects of calculation domain size, the character of the initially imbedded vortex (e.g., Lamb vortex versus a Rankine or Rosenhead vortex), the individual or combined effects of integration time, grid-size, and the boundary conditions be, among the most important computational input parameters.
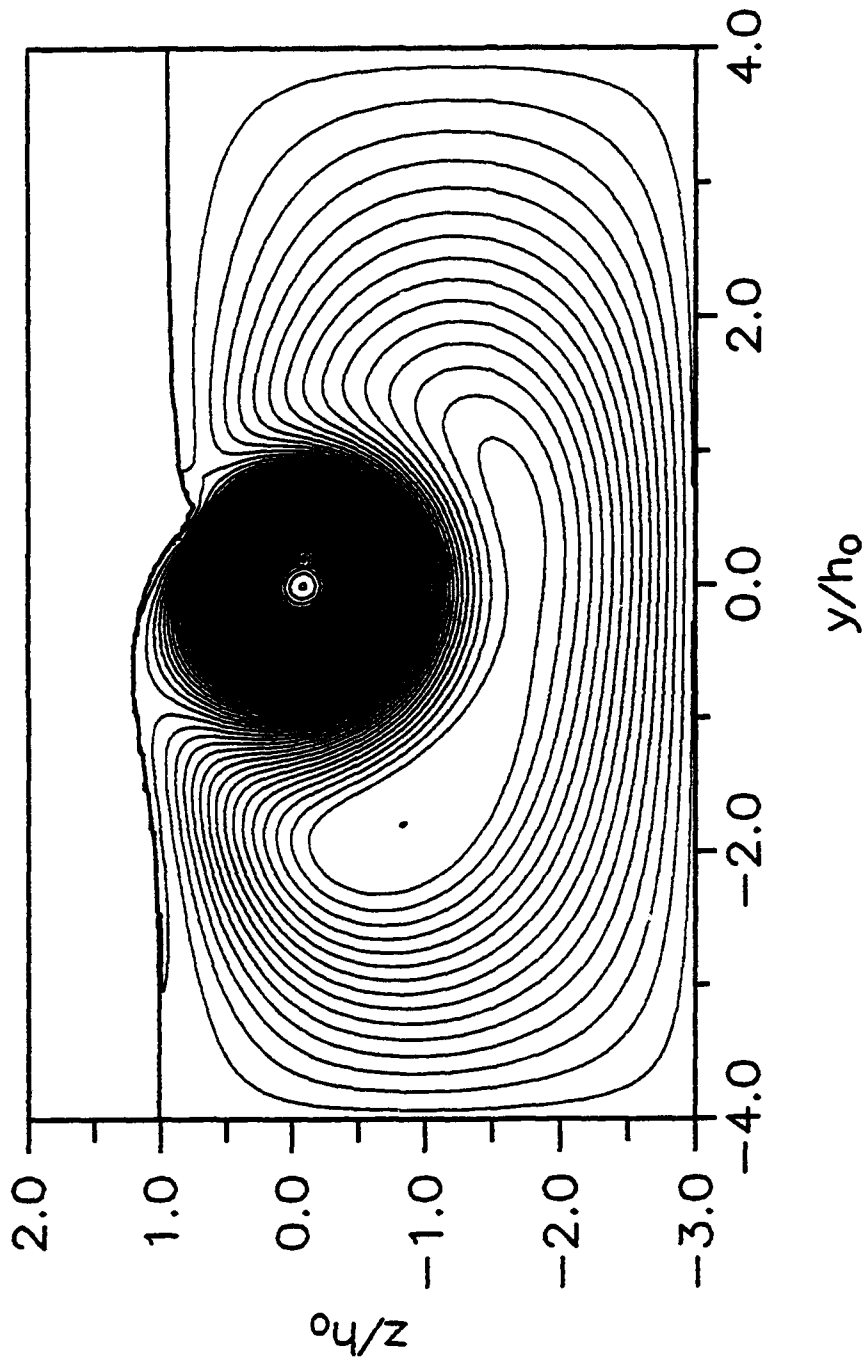
Figure 3. Set #1 Streamlines (Fr = 7.50, Re = 40 and We = 0.033 at T = 27)
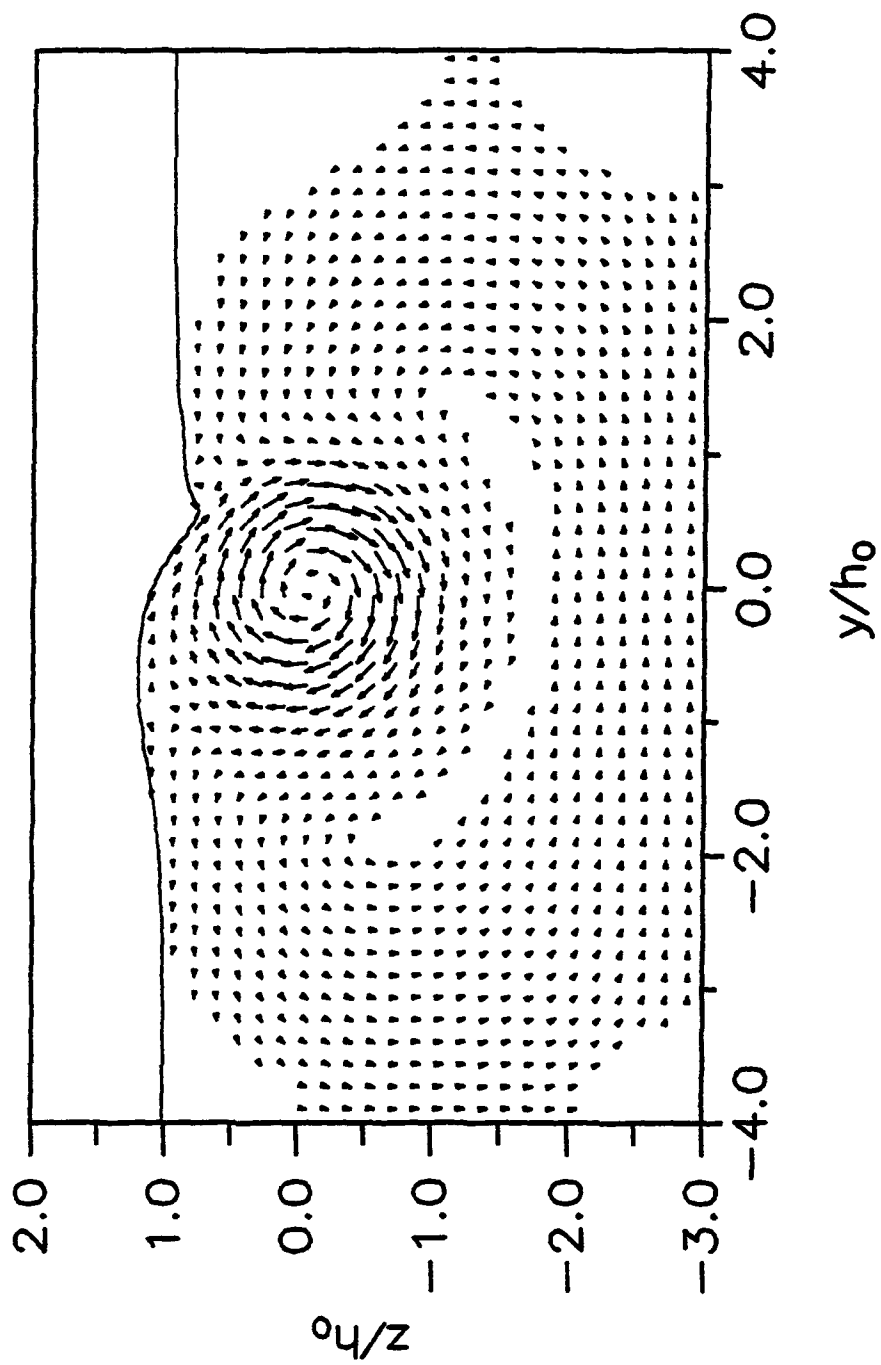
Figure 4.   Set #1 Velocity Vectors (Fr = 7.50, Re = 40 and We = 0.033 at T = 27)
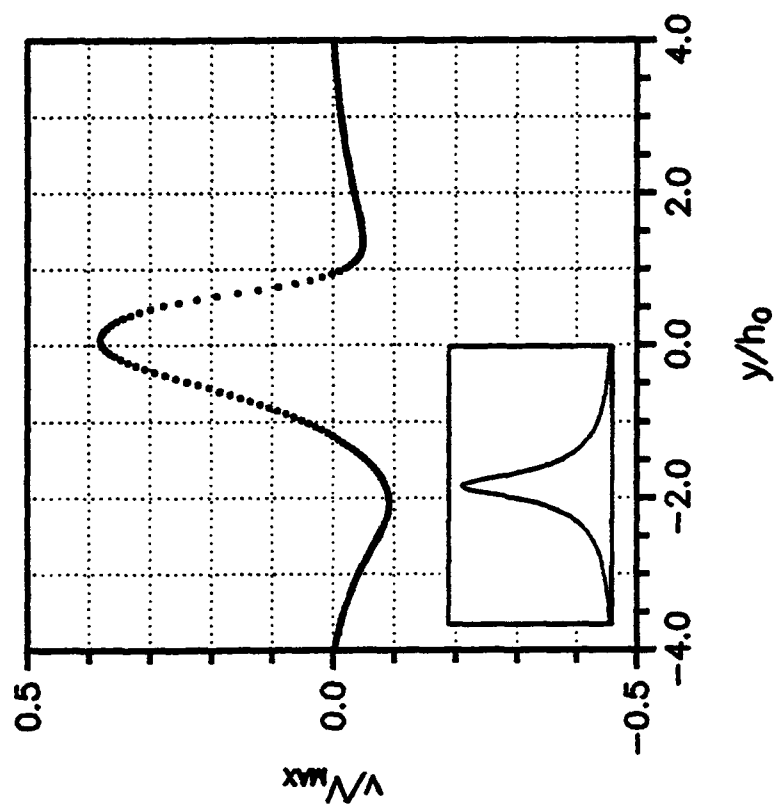
Figure 5. Set #1 v/V_{MAX} versus Transverse Distance at $z/h_o = 0.50$
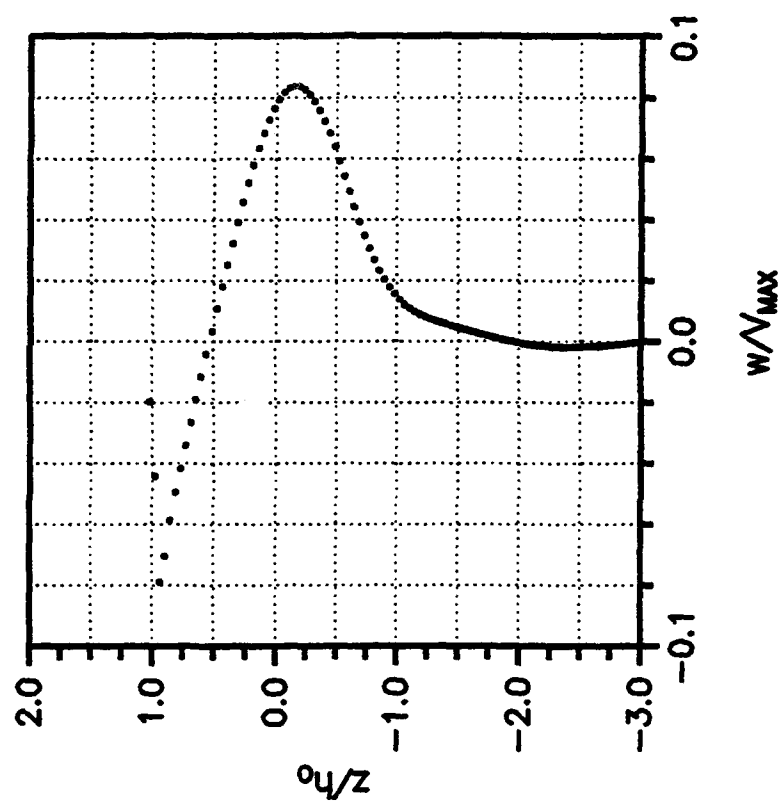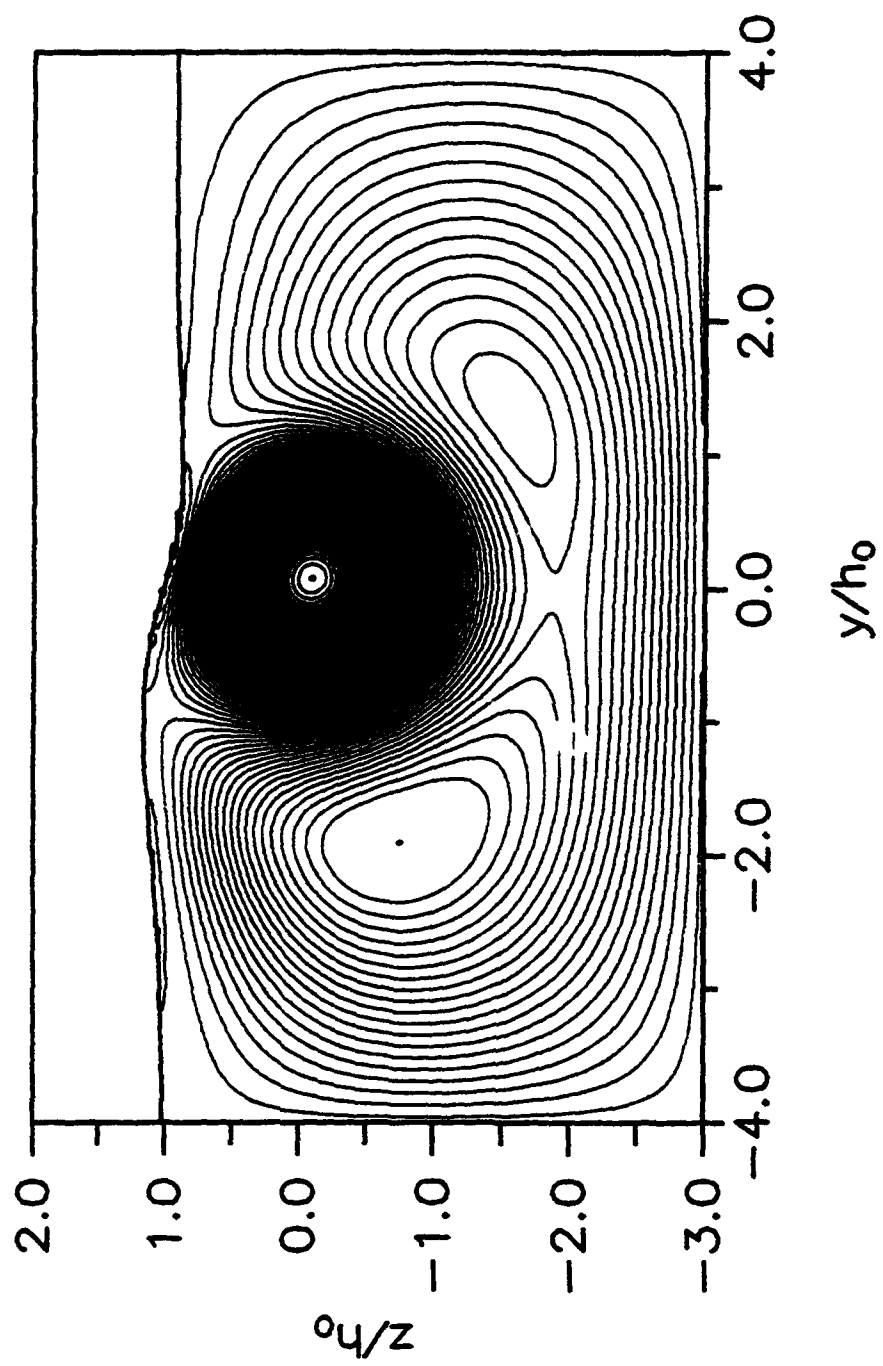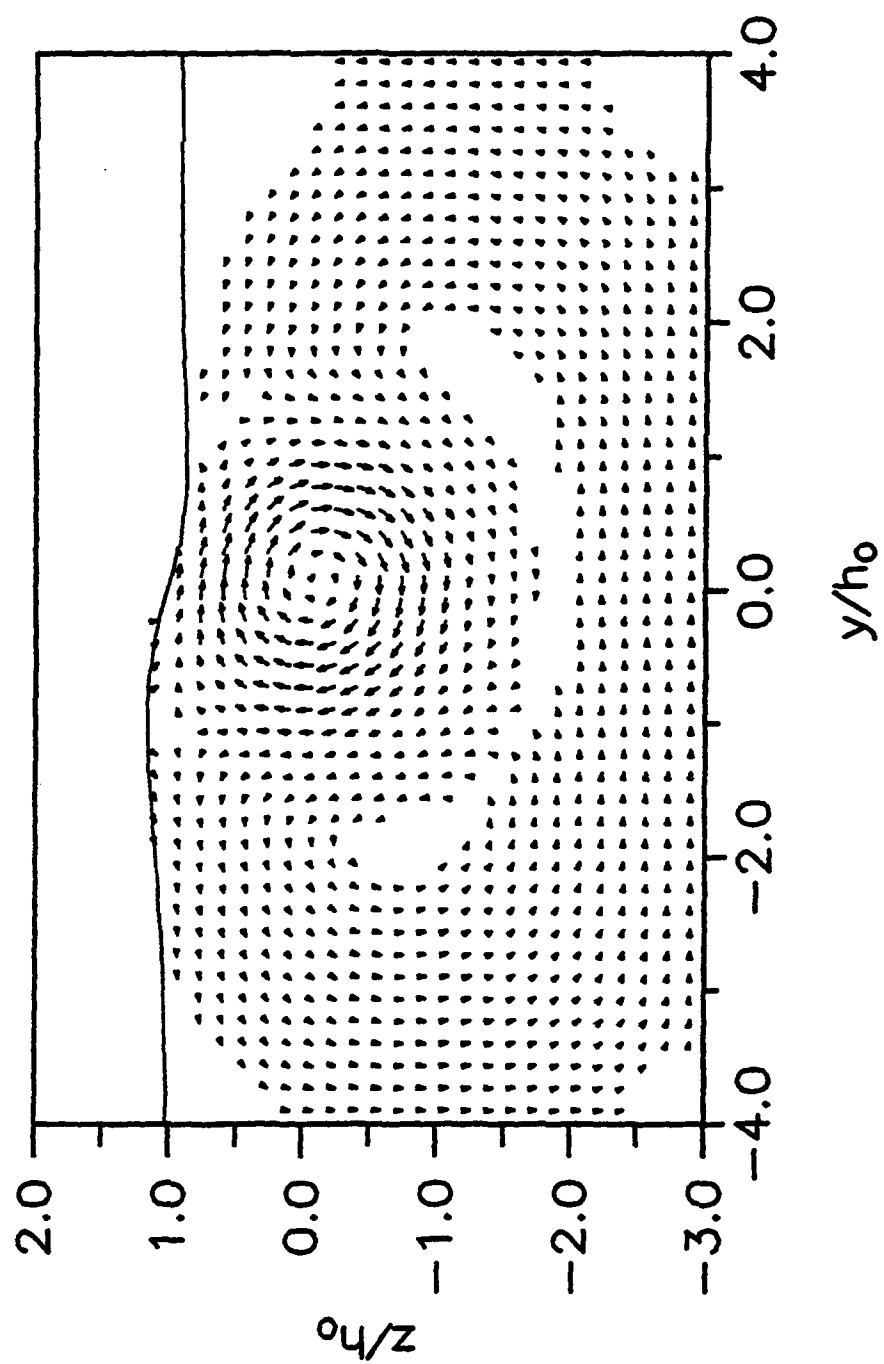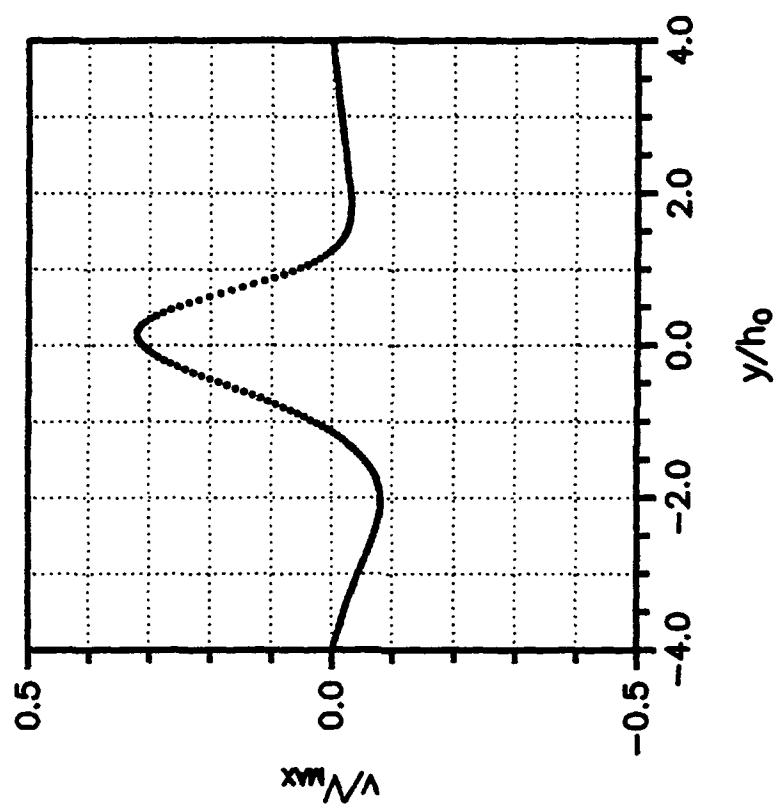
(Fr = 7.50, Re = 40 and We = 0.033 at T = 27)

Figure 6. Set #1 w/V_{MAX} versus Transverse Distance at $z/h_0 = 0.50$

(Fr = 7.50, Re = 40 and We = 0.033 at T = 27)

32
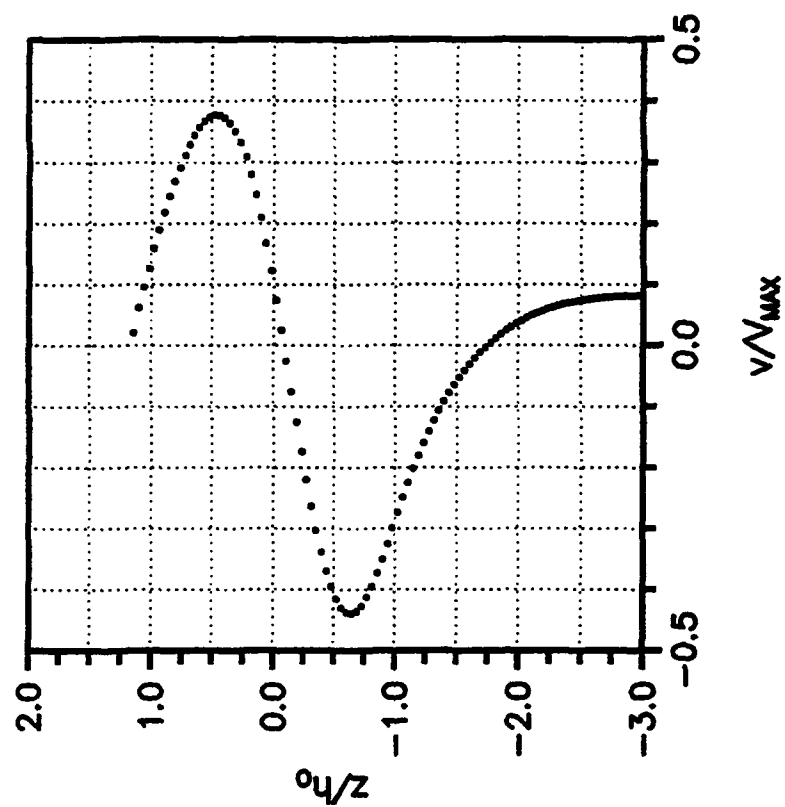
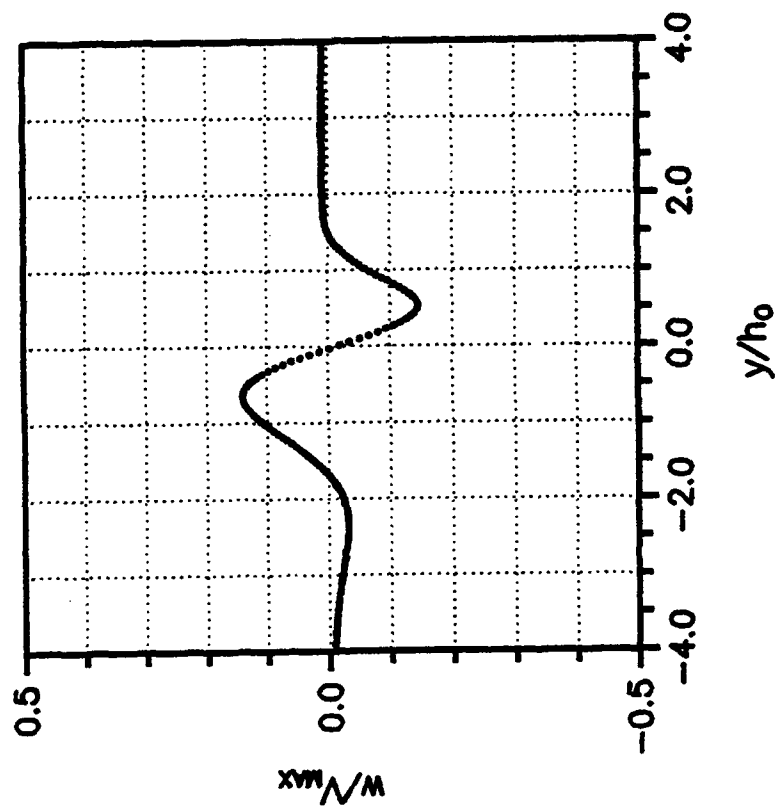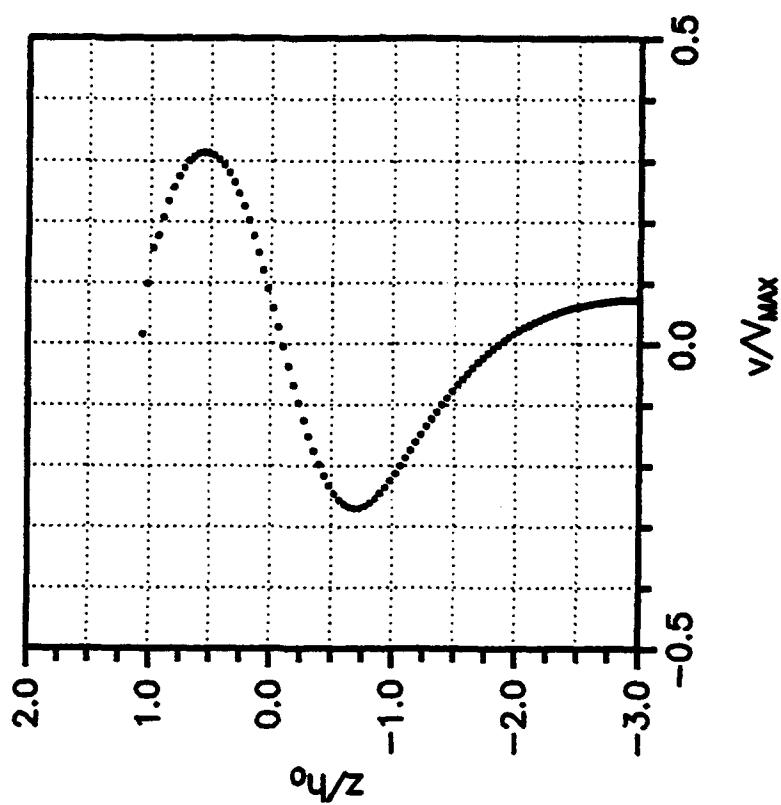Figure 7.   Set #1 v/V_{MAX} versus Vertical Distance at y/h_0 = 0.00
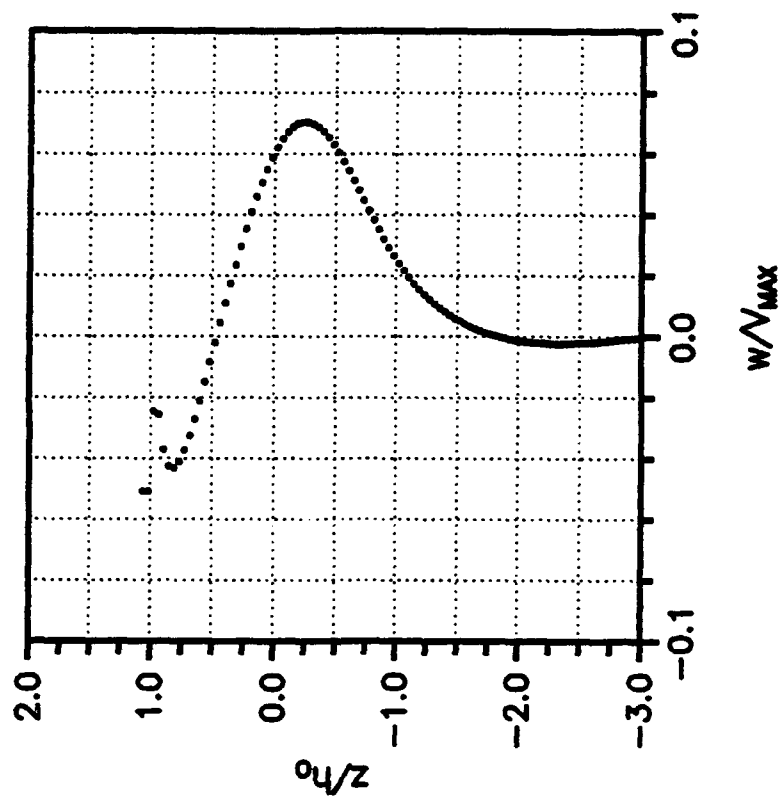
(Fr = 7.50, Re = 40 and We = 0.033 at T = 27)
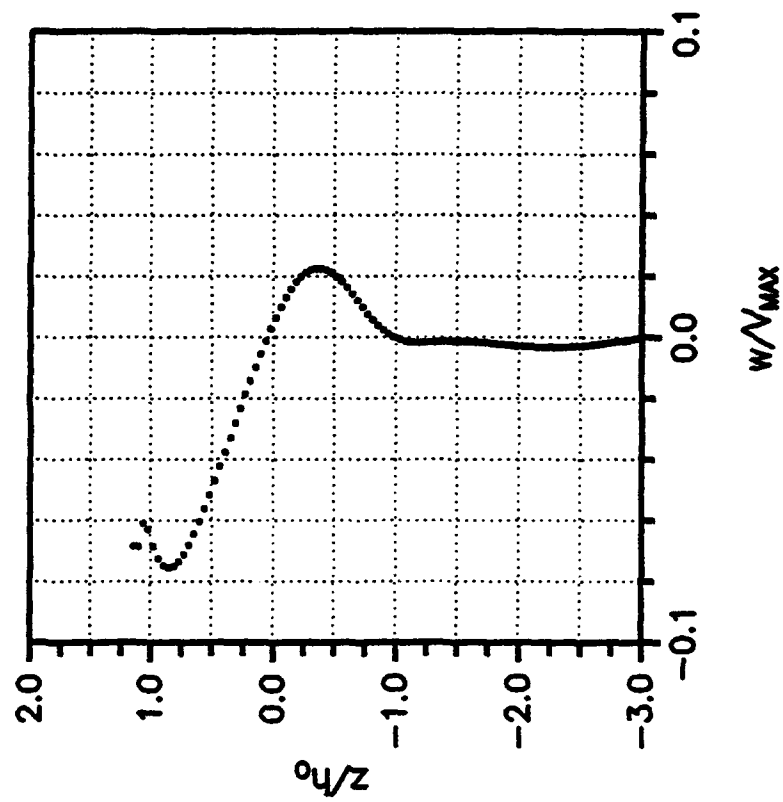
Figure 8. Set #1 w/V_{MAX} versus Vertical Distance at y/h_o = 0.00

(Fr = 7.50, Re = 40 and We = 0.033 at T = 27)

34
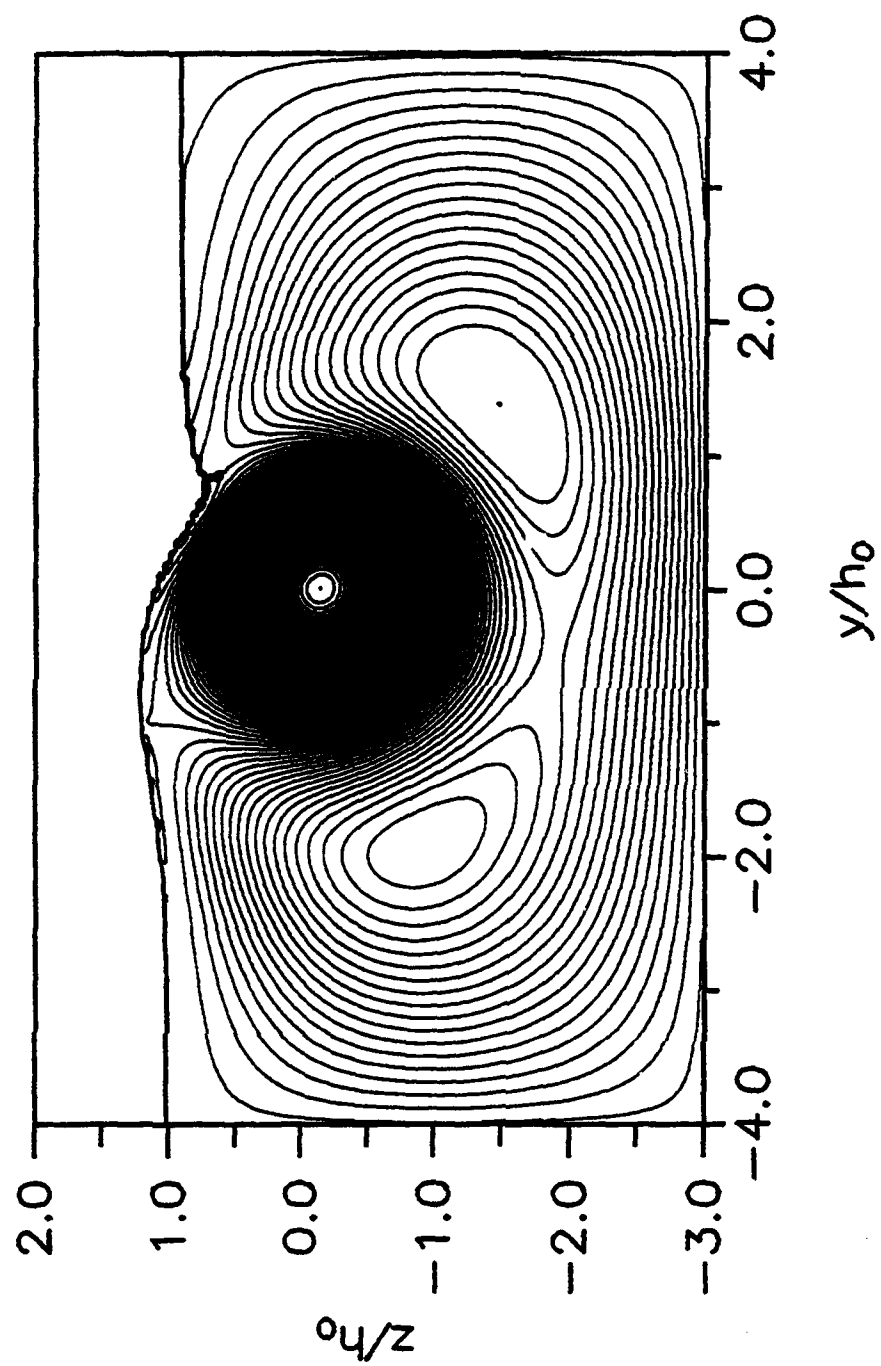
Figure 9.   Set #2 Streamlines (Fr = 7.50, Re = 20 and We = 0.033 at T = 27)

35
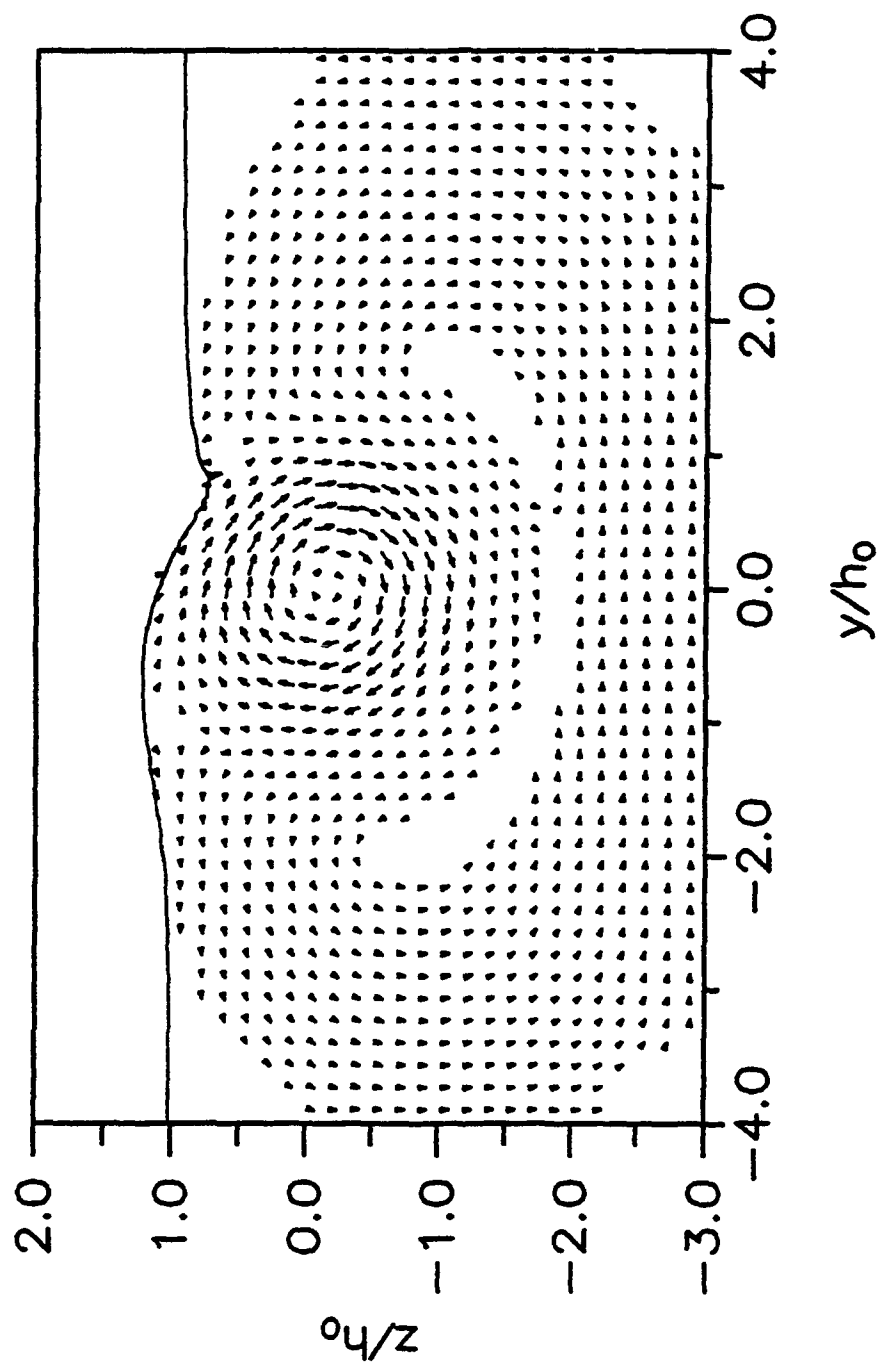
Figure 10.   Set #2 Velocity Vectors (Fr = 7.50, Re = 20 and We = 0.033 at Γ = 27)

36
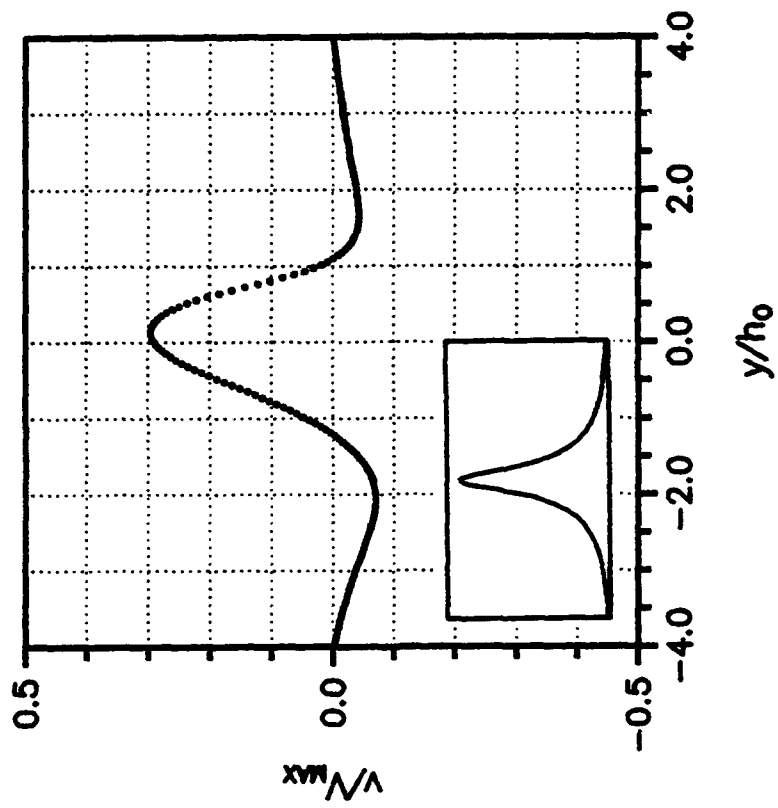
Figure 11. Set #2 v/V_{MAX} versus Transverse Distance at $z/h_o = 0.50$

(Fr = 7.50, Re = 20 and We = 0.033 at T = 27)
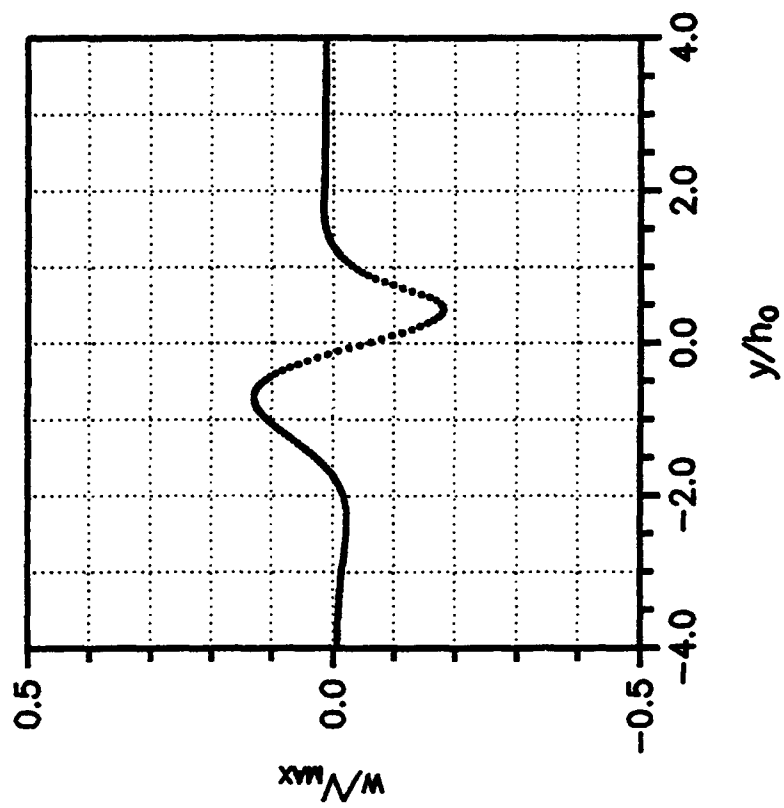
Figure 12.   Set #2 w/V_{MAX} versus Transverse Distance at z/h_o = 0.50

(Fr = 7.50, Re = 20 and We = 0.033 at T = 27)

Figure 13. Set #2 v/V_{MAX} versus Vertical Distance at $y/h_o = 0.00$
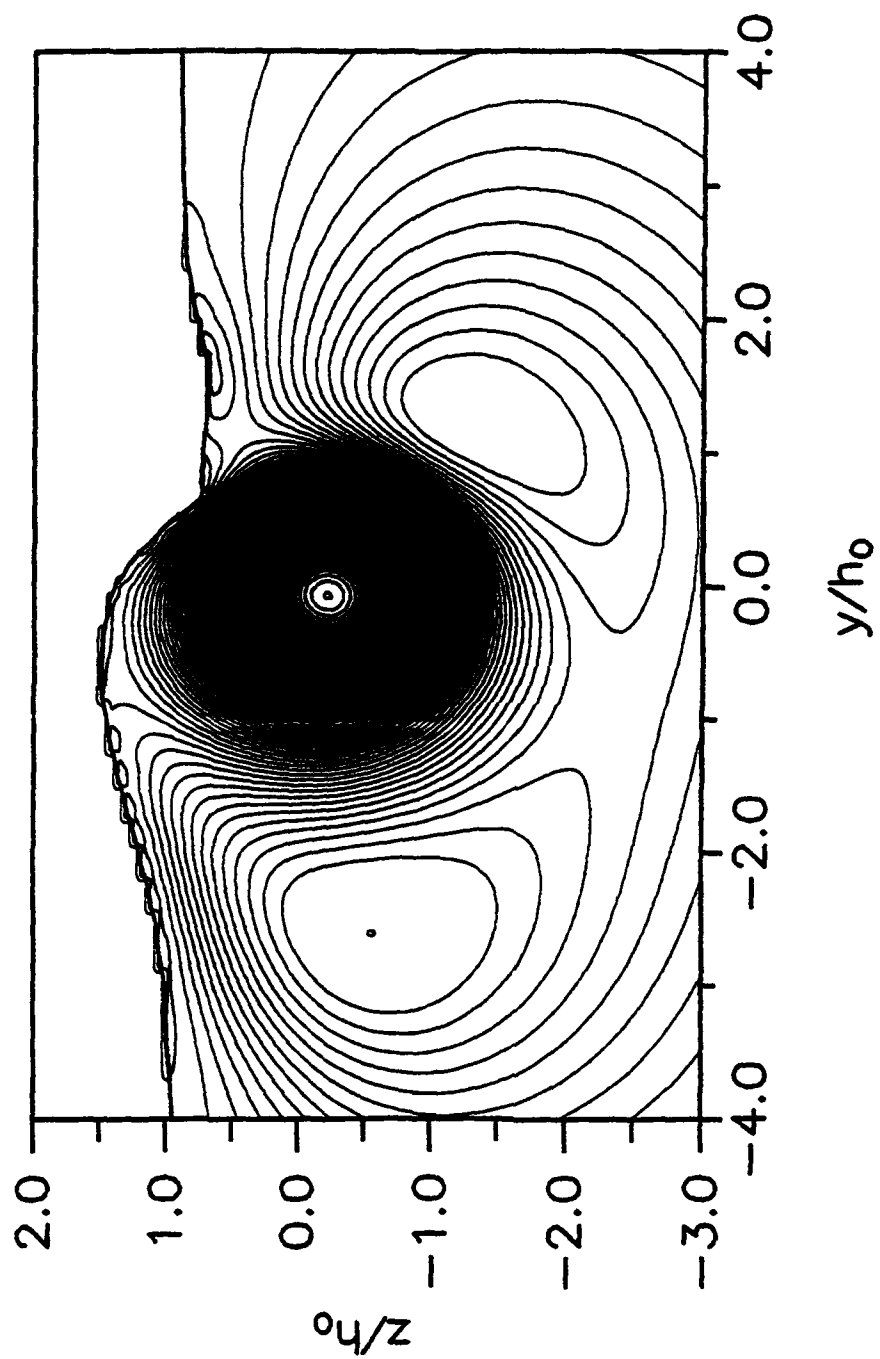
(Fr = 7.50, Re = 20 and We = 0.033 at T = 27)

Figure 14. Set #2 w/V_{MAX} versus Vertical Distance at $y/h_o = 0.00$

(Fr = 7.50, Re = 20 and We = 0.033 at T = 27)

Figure 15. Set #3 Streamlines (Fr = 7.50, Re = 40 and We = 0.333 at T = 27)

41
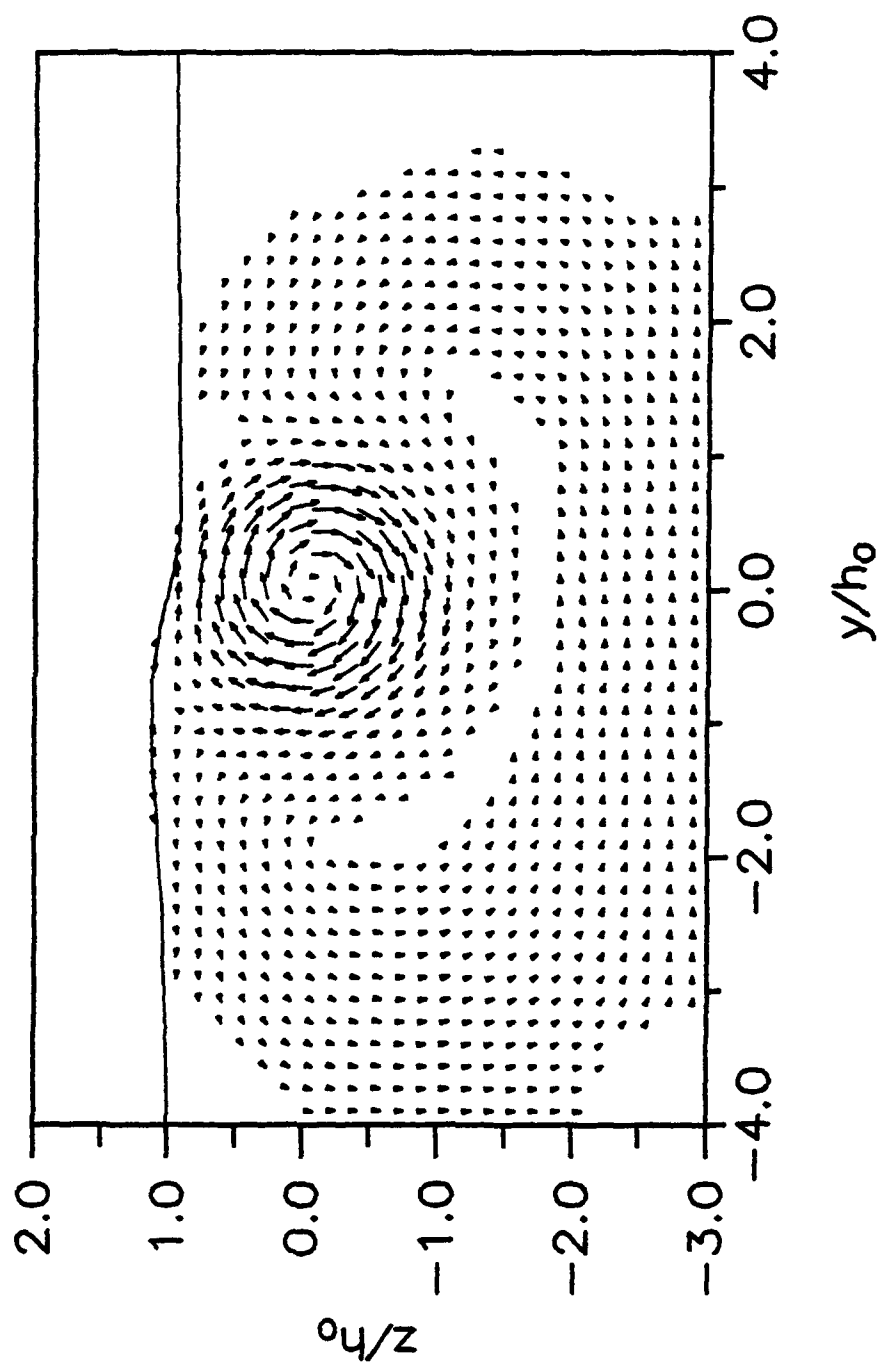
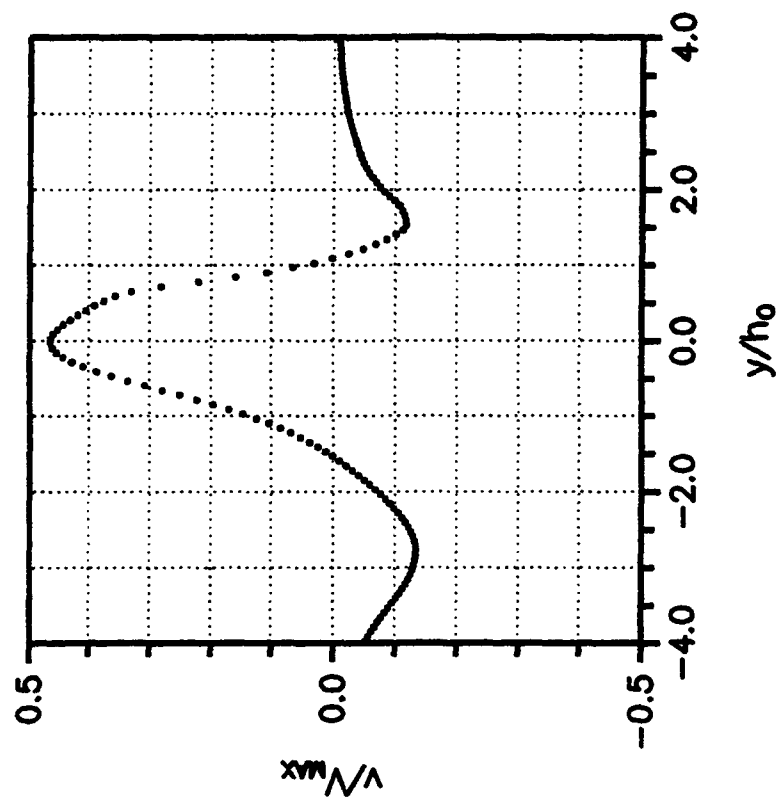Figure 16. Set #3 Velocity Vectors (Fr = 7.50, Re = 40 and We = 0.333 at T = 27)
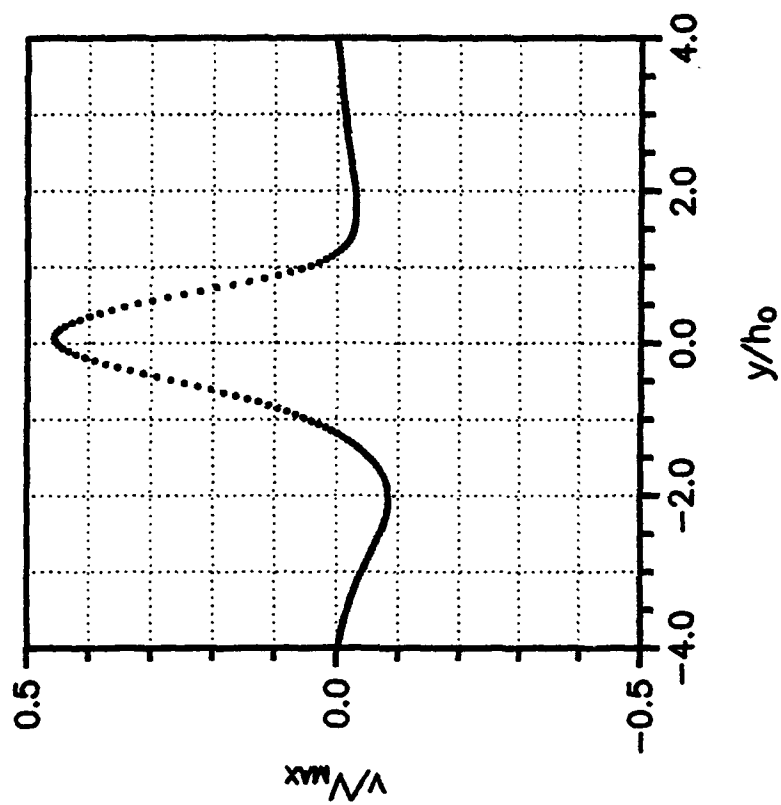
Figure 17. Set #3 v/V_{MAX} versus Transverse Distance at $z/h_o = 0.50$
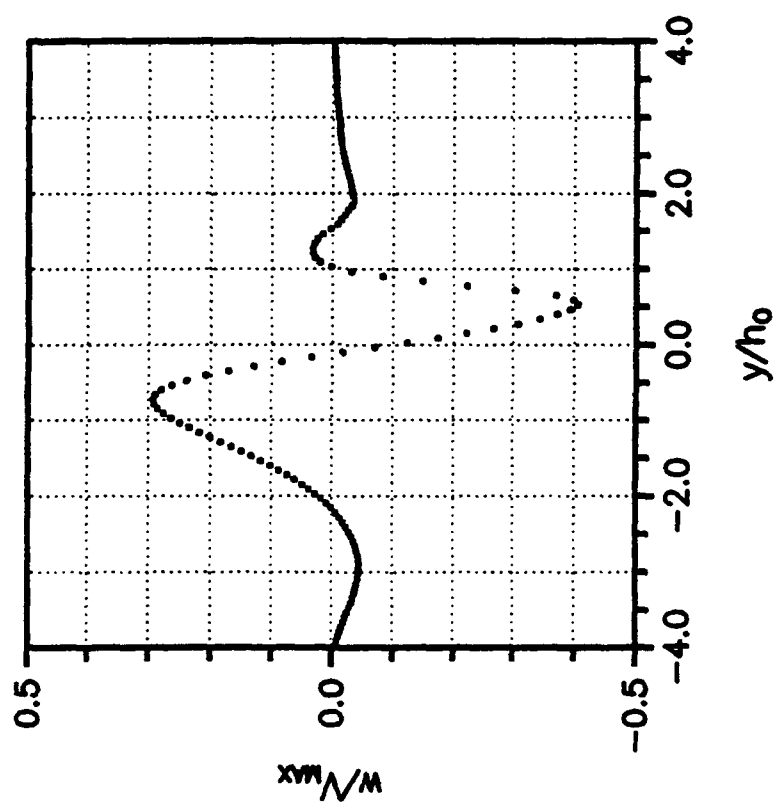
(Fr = 7.50, Re = 40 and We = 0.333 at T = 27)

43

Figure 18. Set #3 w/V_{MAX} versus Transverse Distance at $z/h_o = 0.50$
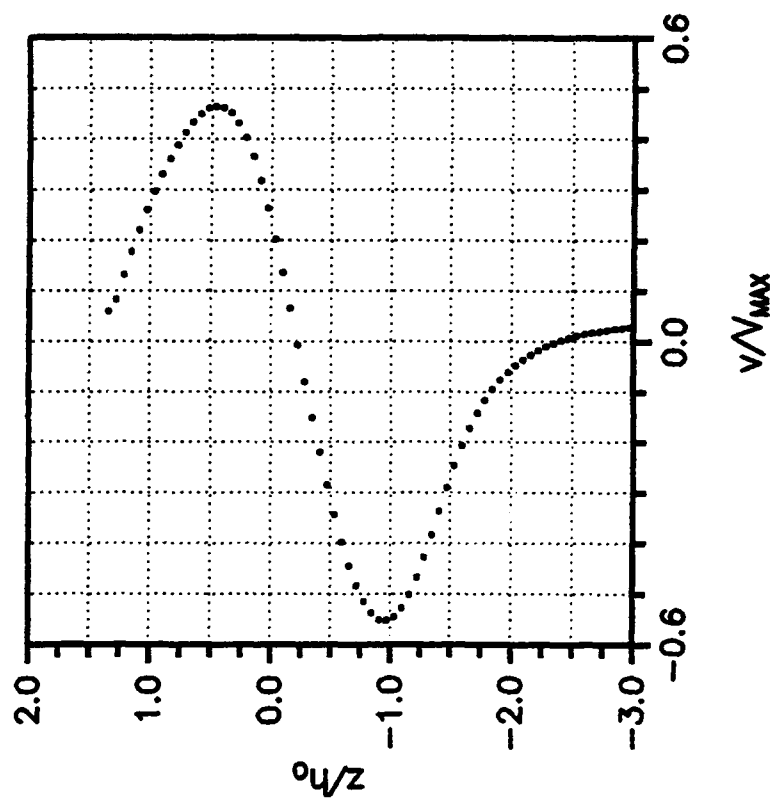
(Fr = 7.50, Re = 40 and We = 0.333 at T = 27)

44

Figure 19. Set #3 v/V_{MAX} versus Vertical Distance at $y/h_o = 0.00$
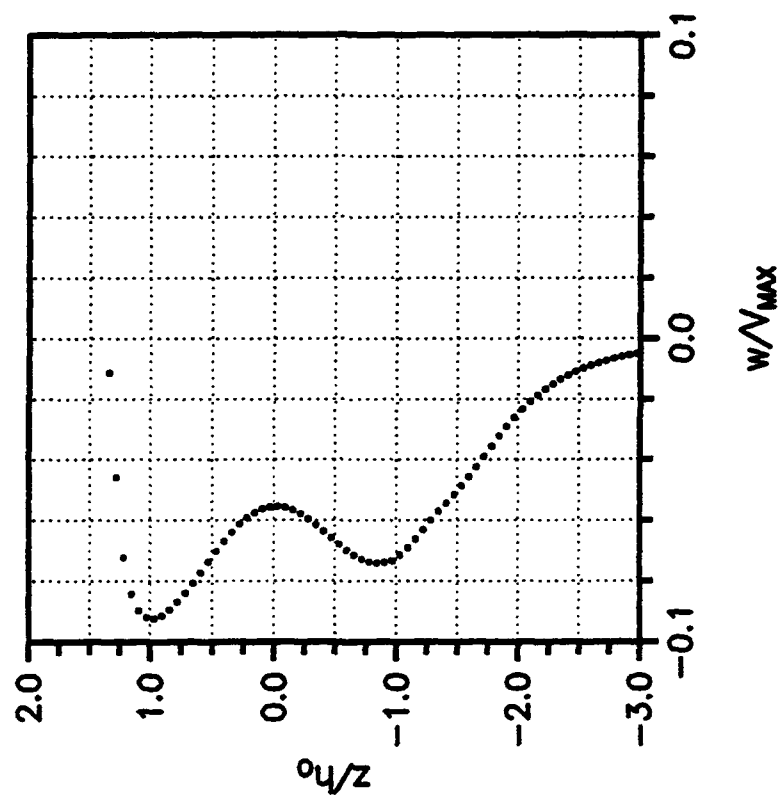
(Fr = 7.50, Re = 40 and We = 0.333 at T = 27)

Figure 20. Set #3 w/V_{MAX} versus Vertical Distance at y/h_o = 0.00

(Fr = 7.50, Re = 40 and We = 0.333 at T = 27)

46

Figure 21. Set #4 Streamlines (Fr = 7.50, Re = 20 and We = 0.333 at T = 27)

Figure 22.   Set #4 Velocity Vectors (Fr = 7.50, Re = 20 and We = 0.333 at T = 27)

48

Figure 23. Set #4 v/V_MAX versus Transverse Distance at $z/h_o = 0.50$

(Fr = 7.50, Re = 20 and We = 0.333 at T = 27)

Figure 24.   Set #4 w/V_{MAX} versus Transverse Distance at $z/h_o = 0.50$

(Fr = 7.50, Re = 20 and We = 0.333 at T = 27)

Figure 25. Set #4 v/V_{MAX} versus Vertical Distance at $y/h_o = 0.00$
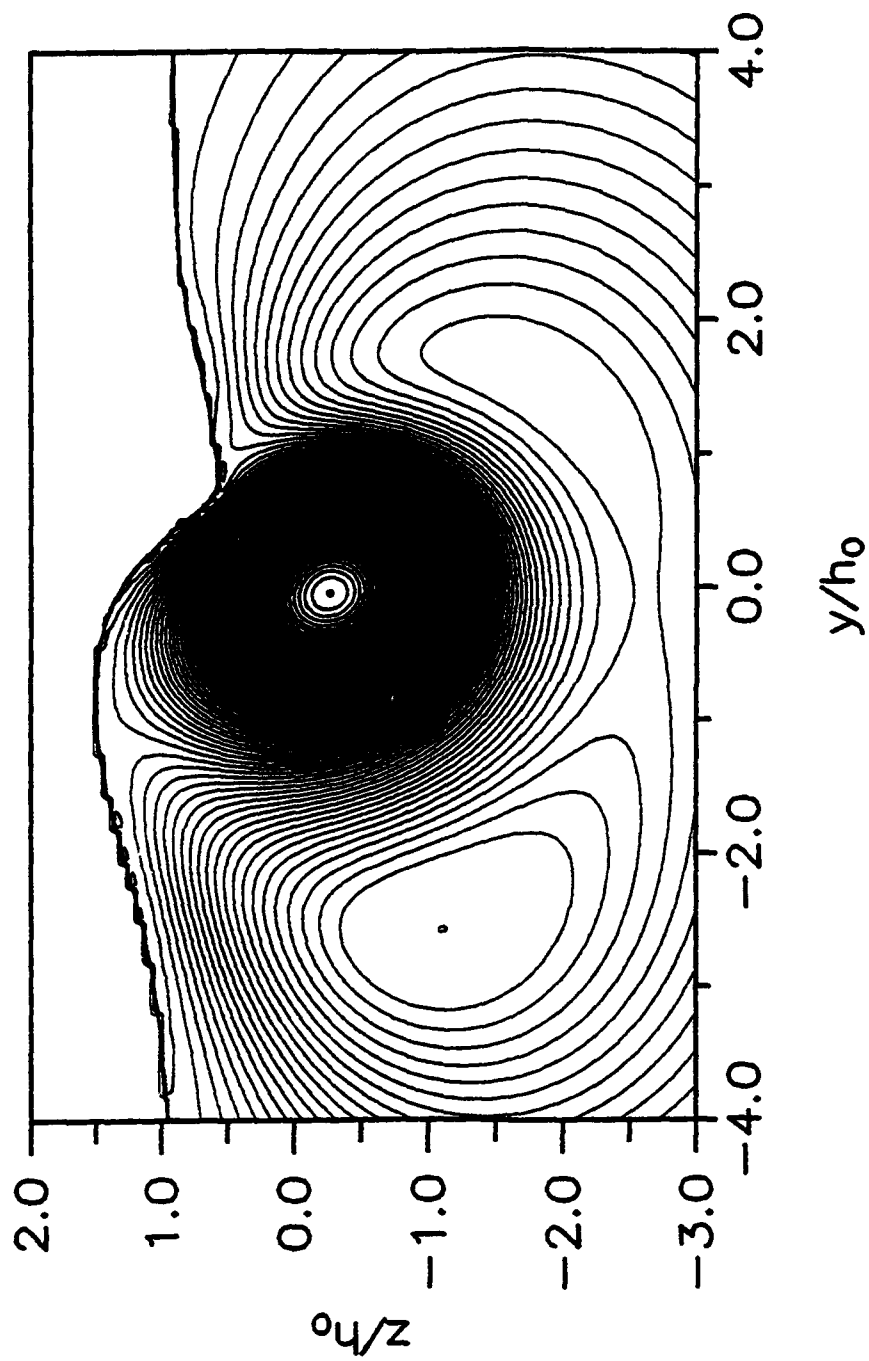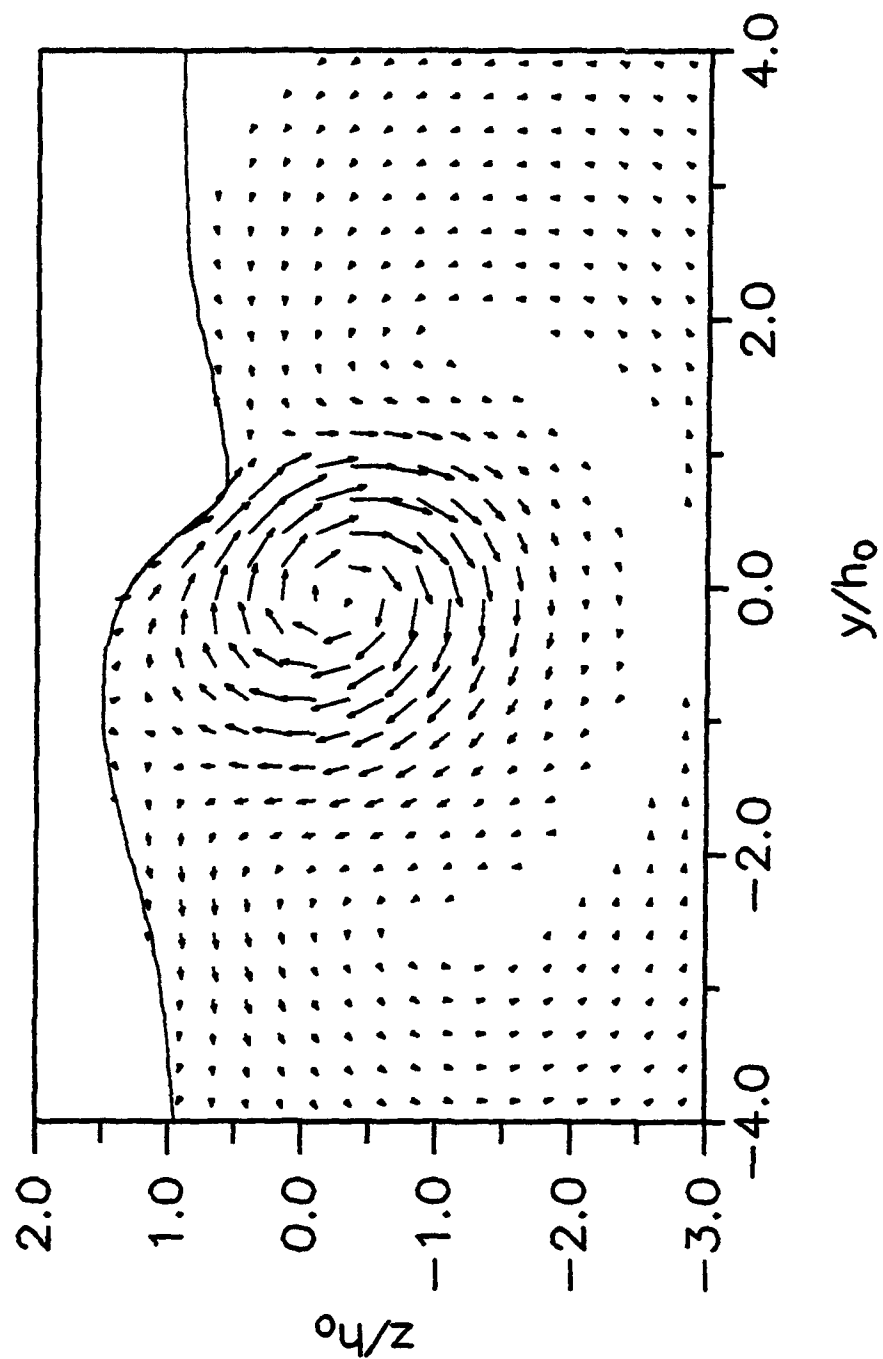
(Fr = 7.50, Re = 20 and We = 0.333 at T = 27)

51

Figure 26. Set #4 w/V_{MAX} versus Vertical Distance at $y/h_o = 0.00$

(Fr = 7.50, Re = 20 and We = 0.333 at T = 27)

52

Figure 27. Set #5 Streamlines (Fr = 13.80, Re = 40 and We = 0.333 at T = 27)
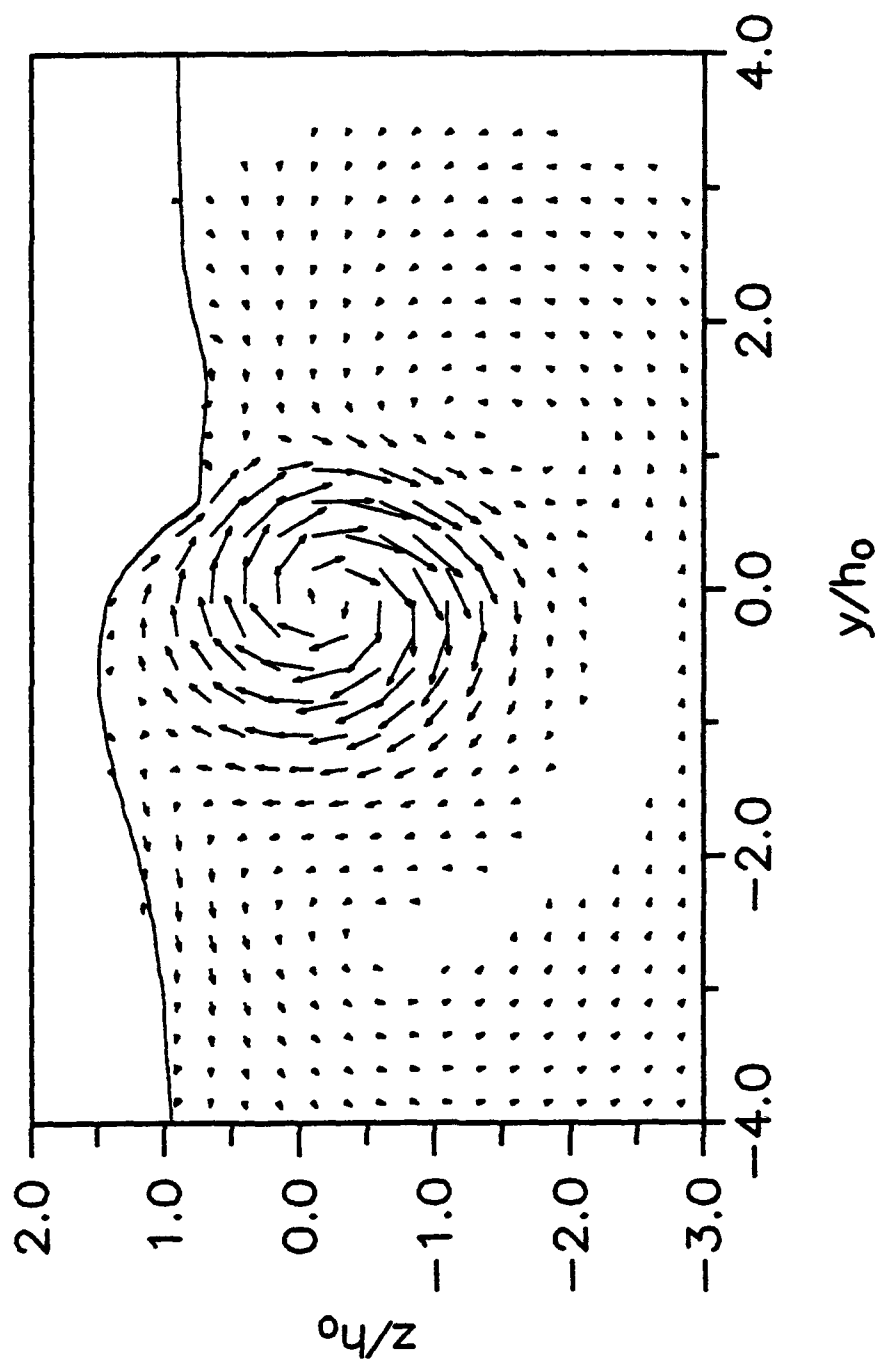
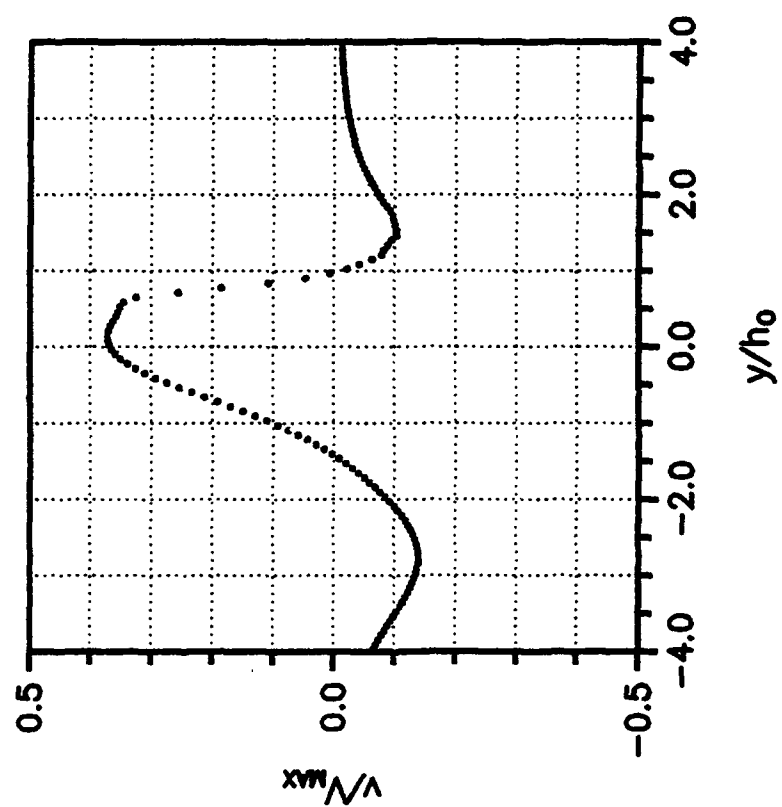Figure 28.   Set #5 Velocity Vectors (Fr = 13.80, Re = 40 and We = 0.333 at T = 27)

Figure 29.   Set #5 v/V $_{MAX}$ versus Transverse Distance at z/h$_o$ = 0.50

(Fr = 13.80, Re = 40 and We = 0.333 at T = 27)

Figure 30. Set #5 w/V_{MAX} versus Transverse Distance at $z/h_o = 0.50$
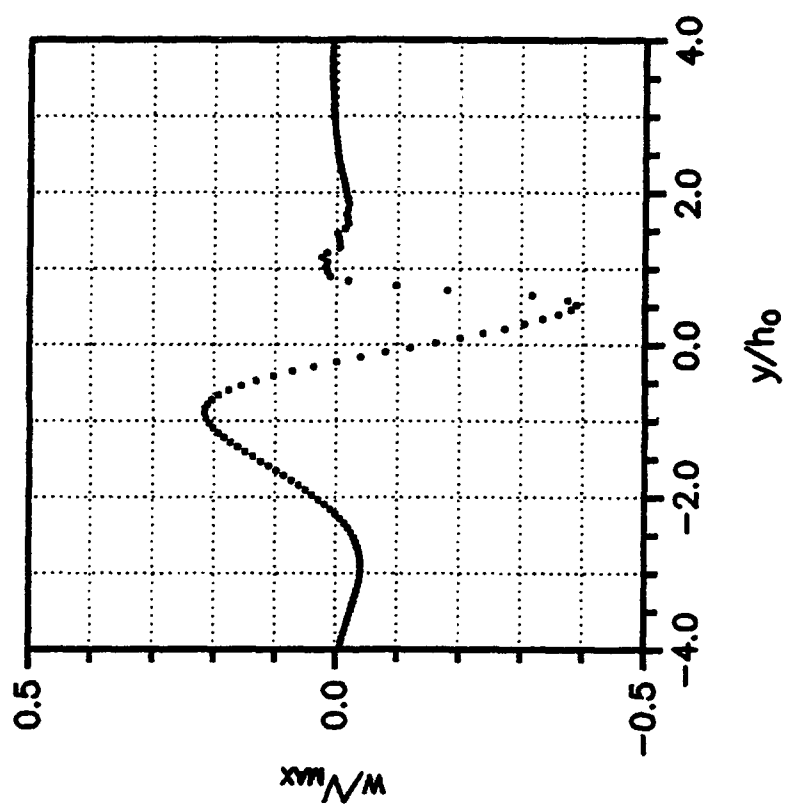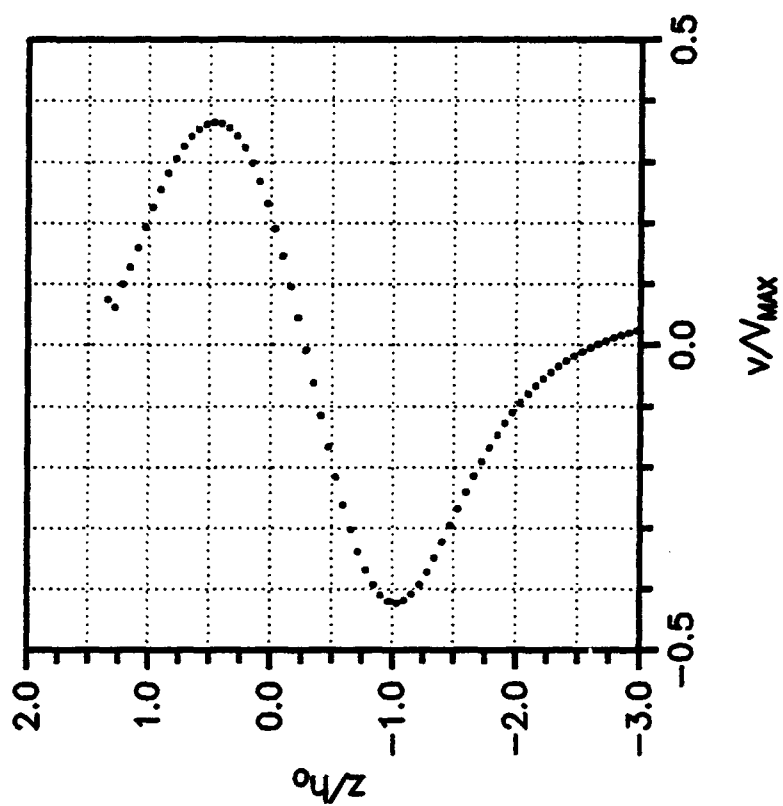
(Fr = 13.80, Re = 40 and We = 0.333 at T = 27)

56

Figure 31. Set #5 v/V$_{MAX}$ versus Vertical Distance at y/h$_o$ = 0.00

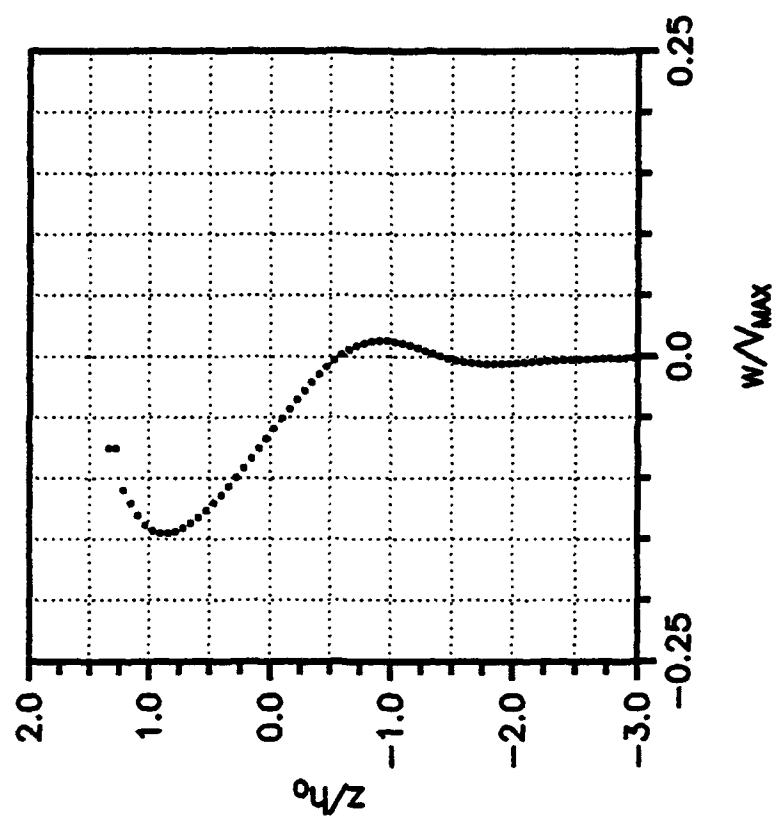(Fr = 13.80, Re = 40 and We = 0.333 at T = 27)

Figure 32.   Set #5 w/V_{MAX} versus Vertical Distance at y/h_o = 0.00

(Fr = 13.80, Re = 40 and We = 0.333 at T = 27)

58

Figure 33. Set #6 Streamlines (Fr = 13.80, Re = 20 and We = 0.333 at T = 27)

59

Figure 34. Set #6 Velocity Vectors (Fr = 13.80, Re = 20 and We = 0.333 at T = 27)

Figure 35. Set #6 v/V$_{MAX}$ versus Transverse Distance at z/h$_o$ = 0.50

(Fr = 13.80, Re = 20 and We = 0.333 at T = 27)

Figure 36.   Set #6 w/V_{MAX} versus Transverse Distance at z/h_o = 0.50

(Fr = 13.80, Re = 20 and We = 0.333 at T = 27)

62

Figure 37. Set #6 v/V$_{MAX}$ versus Vertical Distance at y/h$_o$ = 0.00
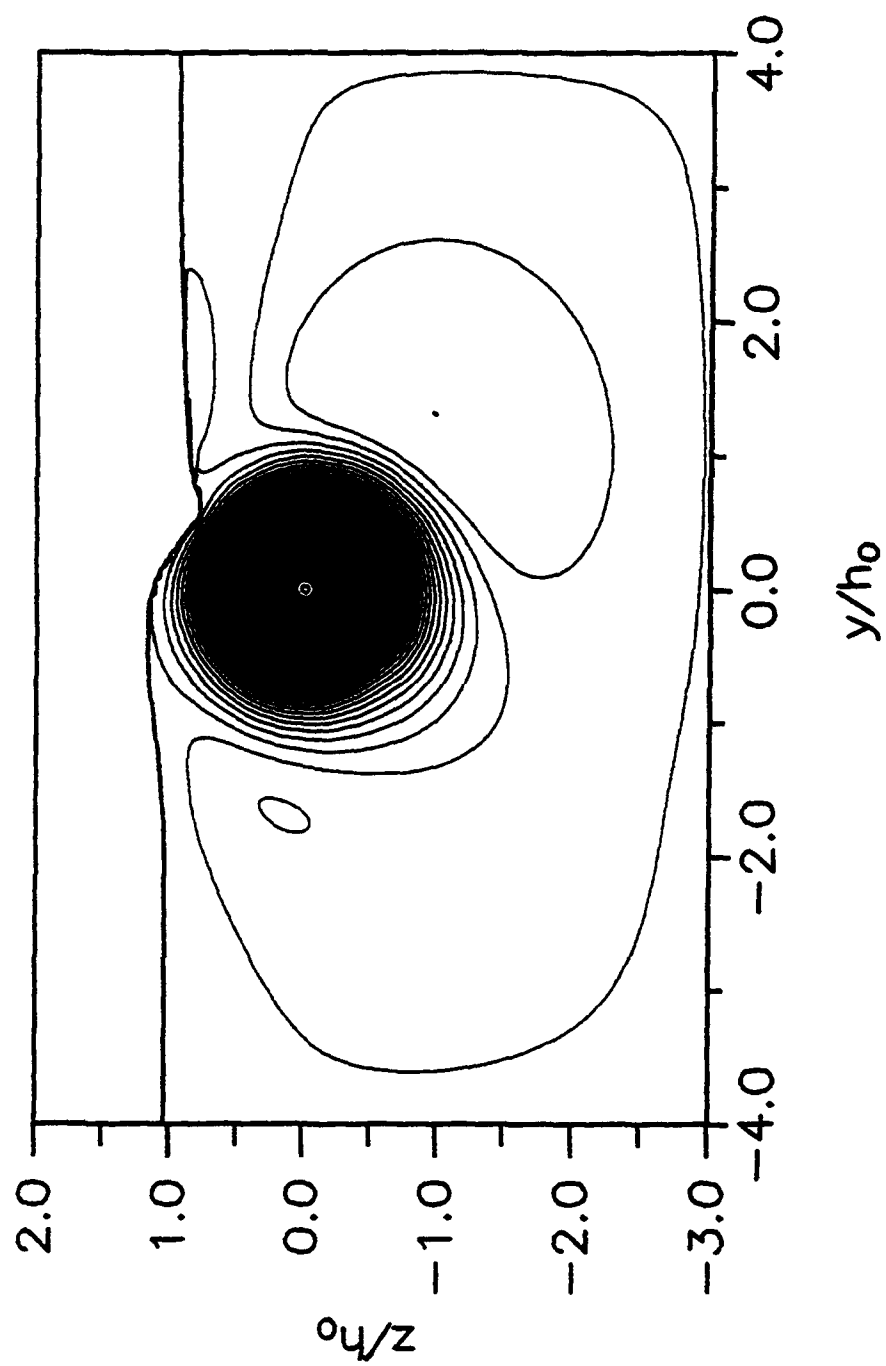
(Fr = 13.80, Re = 20 and We = 0.333 at T = 27)

Figure 38. Set #6 w/V_{MAX} versus Vertical Distance at y/h_o = 0.00

(Fr = 13.80, Re = 20 and We = 0.333 at T = 27)

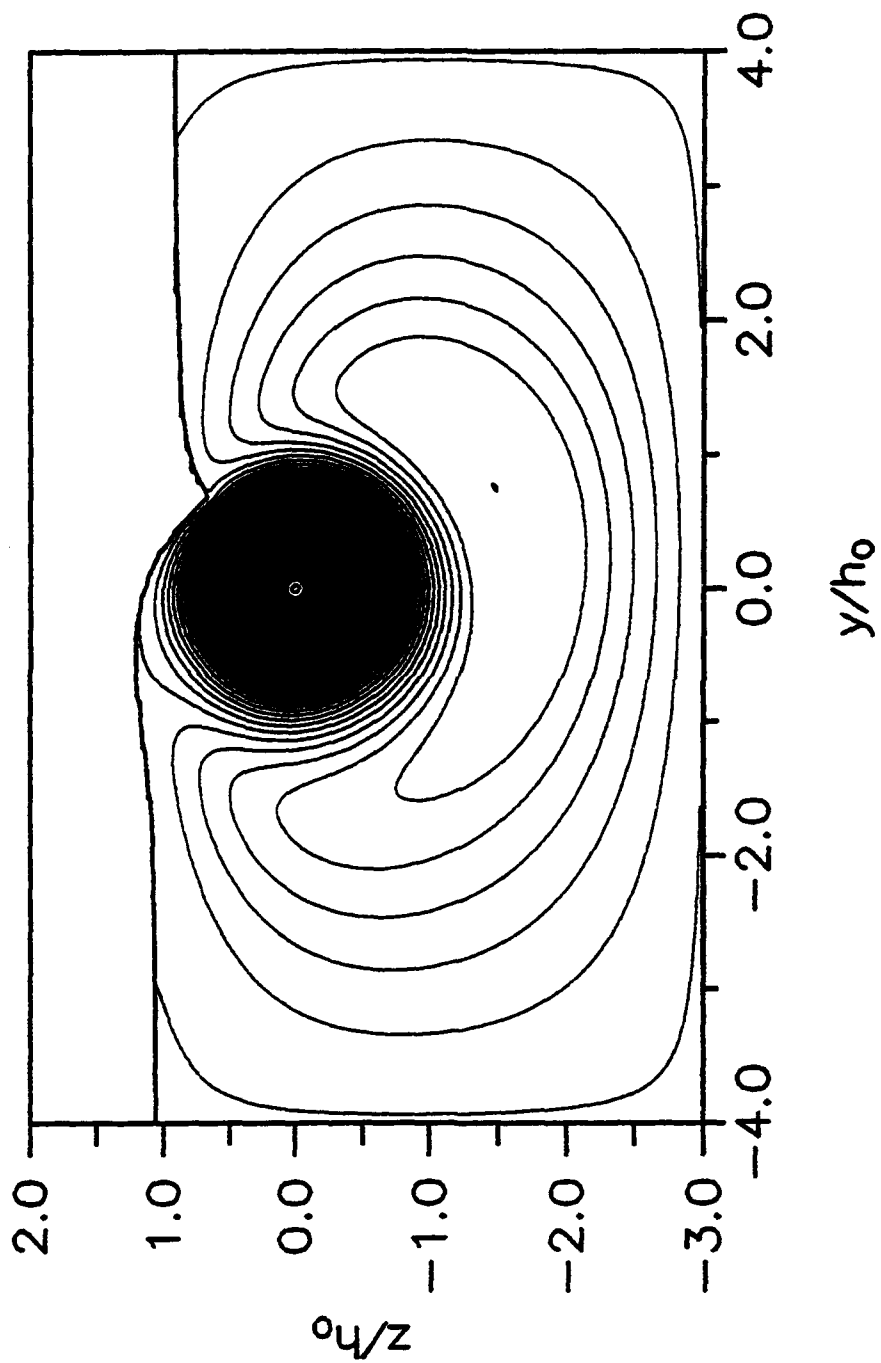Figure 39. Streamlines at T = 10 (Fr = 7.50, Re = 40 and We = 0.033)

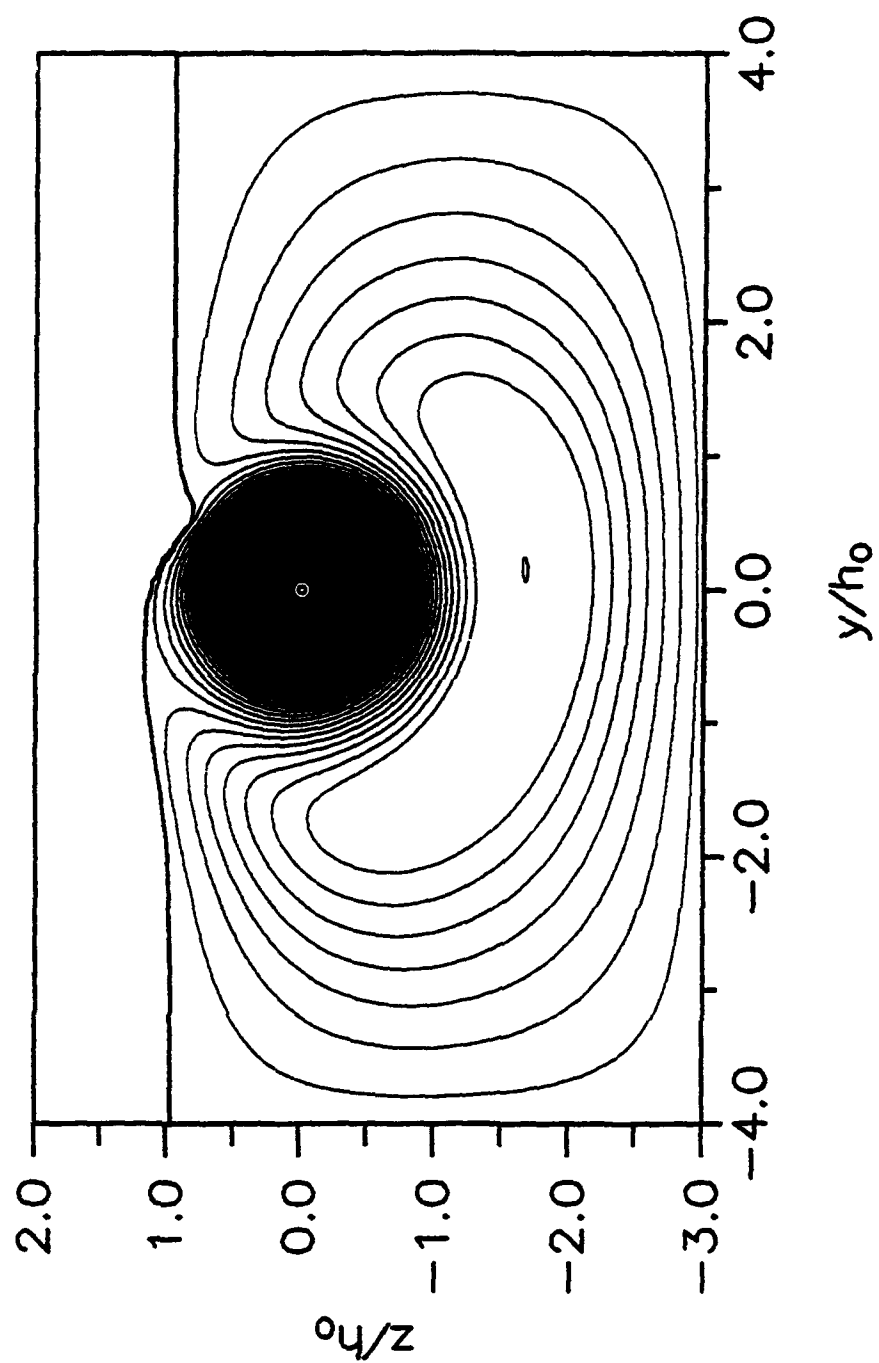Figure 40.   Streamlines at T = 15 (Fr = 7.50, Re = 40 and We = 0.033)

66

Figure 41. Streamlines at T = 20 (Fr = 7.50, Re = 40 and We = 0.033)

67
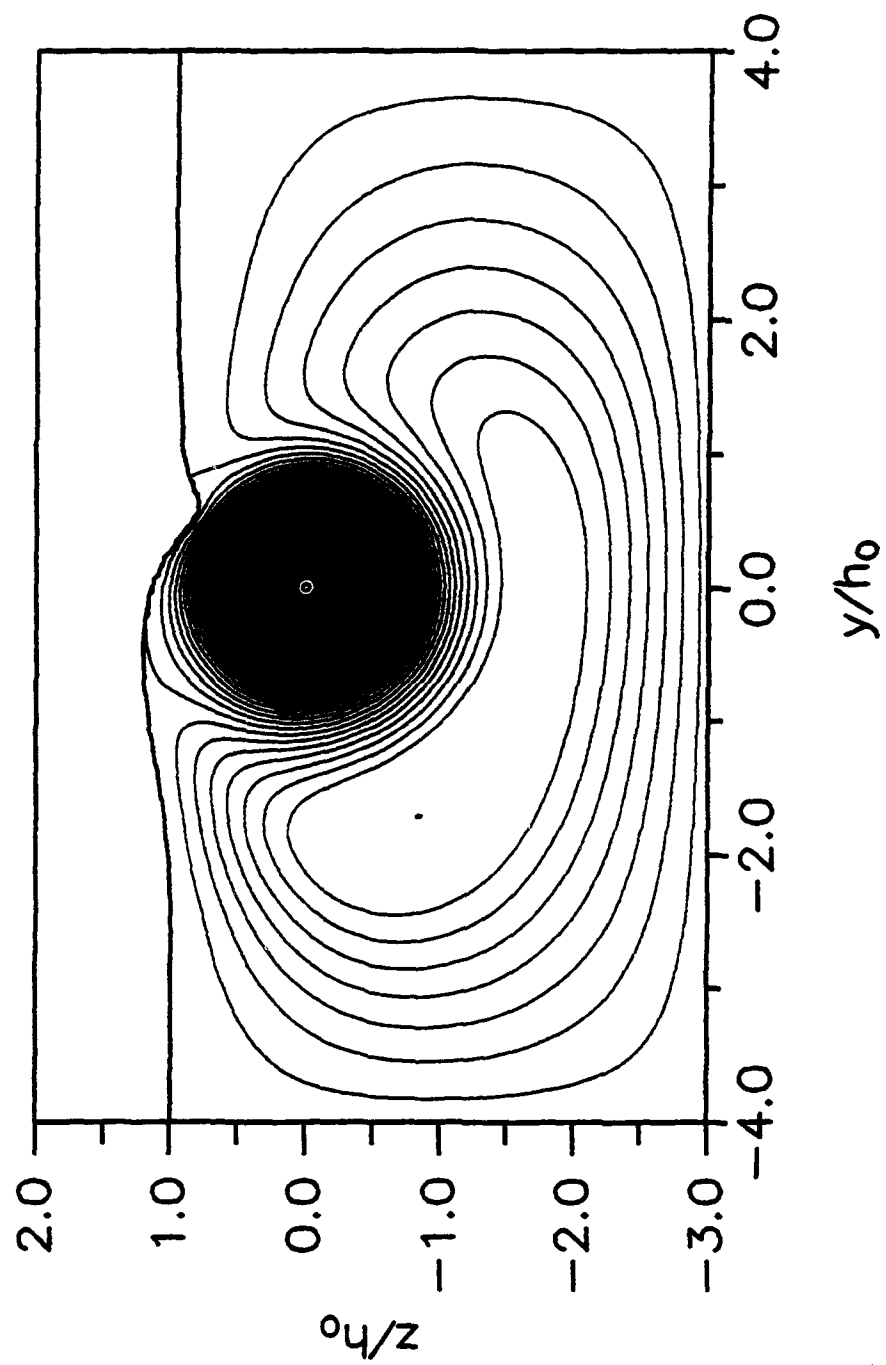
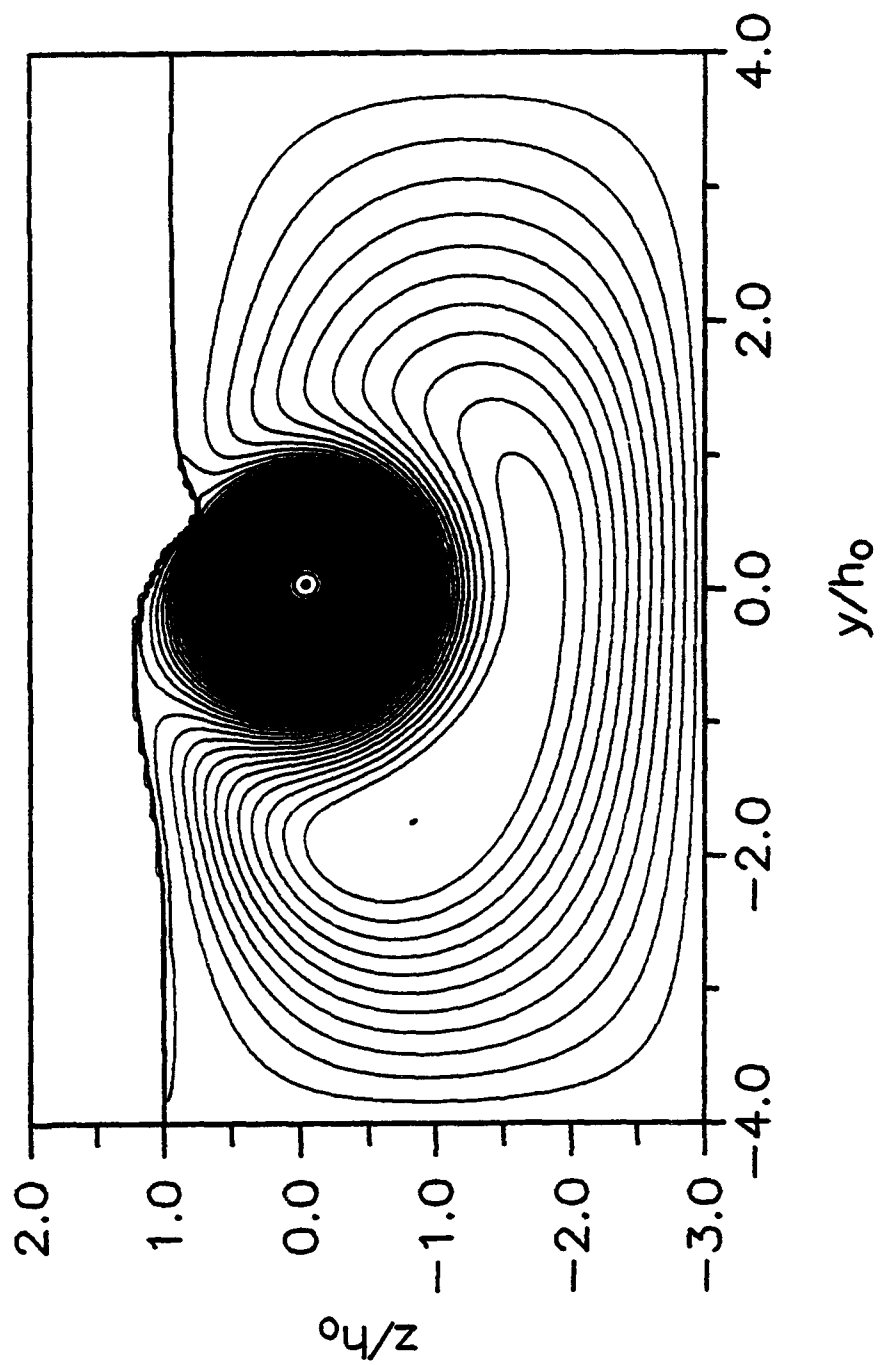Figure 42.   Streamlines at T = 25 (Fr = 7.50, Re = 40 and We = 0.033)

68

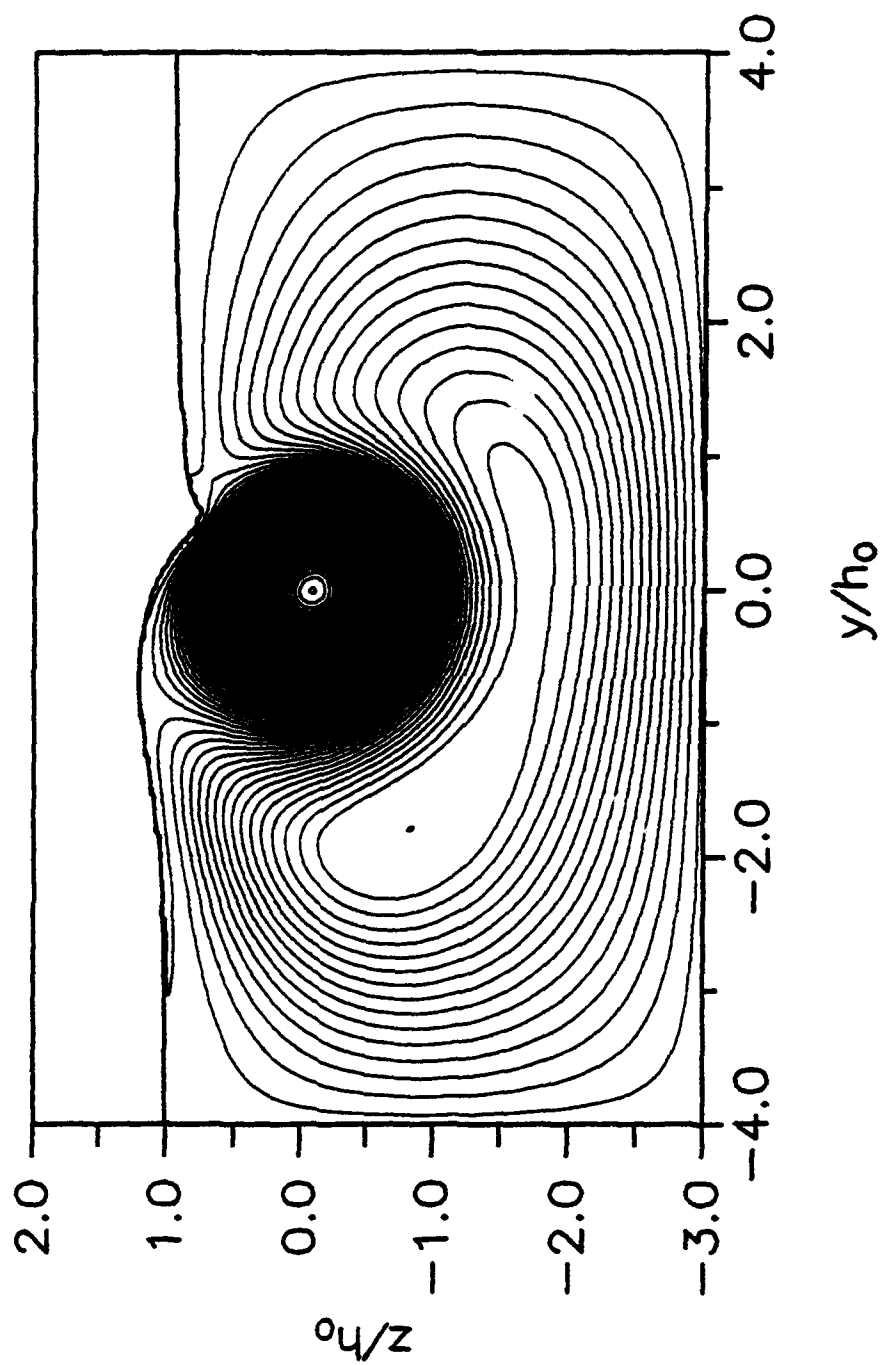Figure 43.   Streamlines at T = 26 (Fr = 7.50, Re = 40 and We = 0.033)

Figure 44.   Streamlines at T = 27 (Fr = 7.50, Re = 40 and We = 0.033)

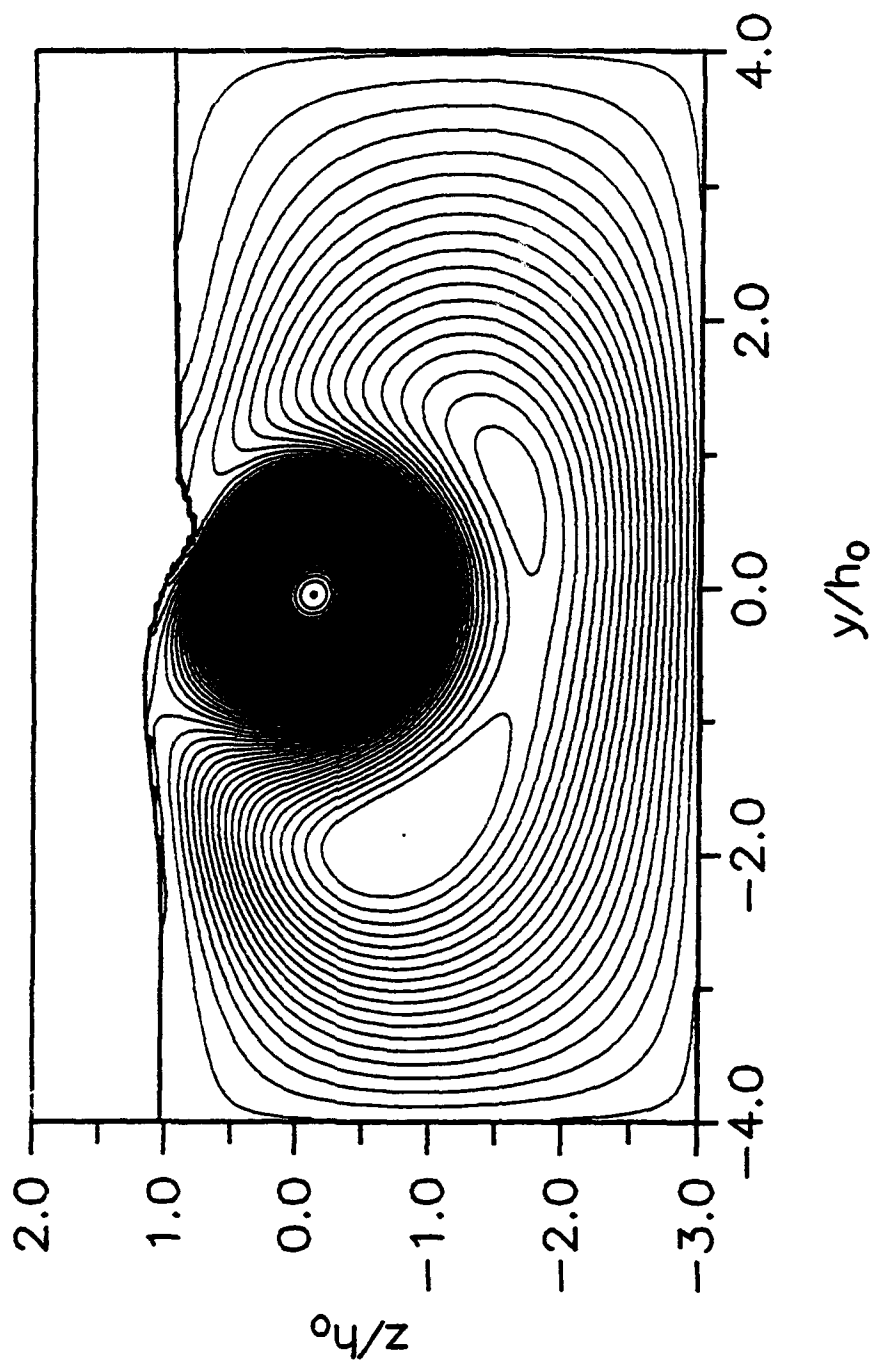Figure 45. Streamlines at T = 28 (Fr = 7.50, Re = 40 and We = 0.033)

71

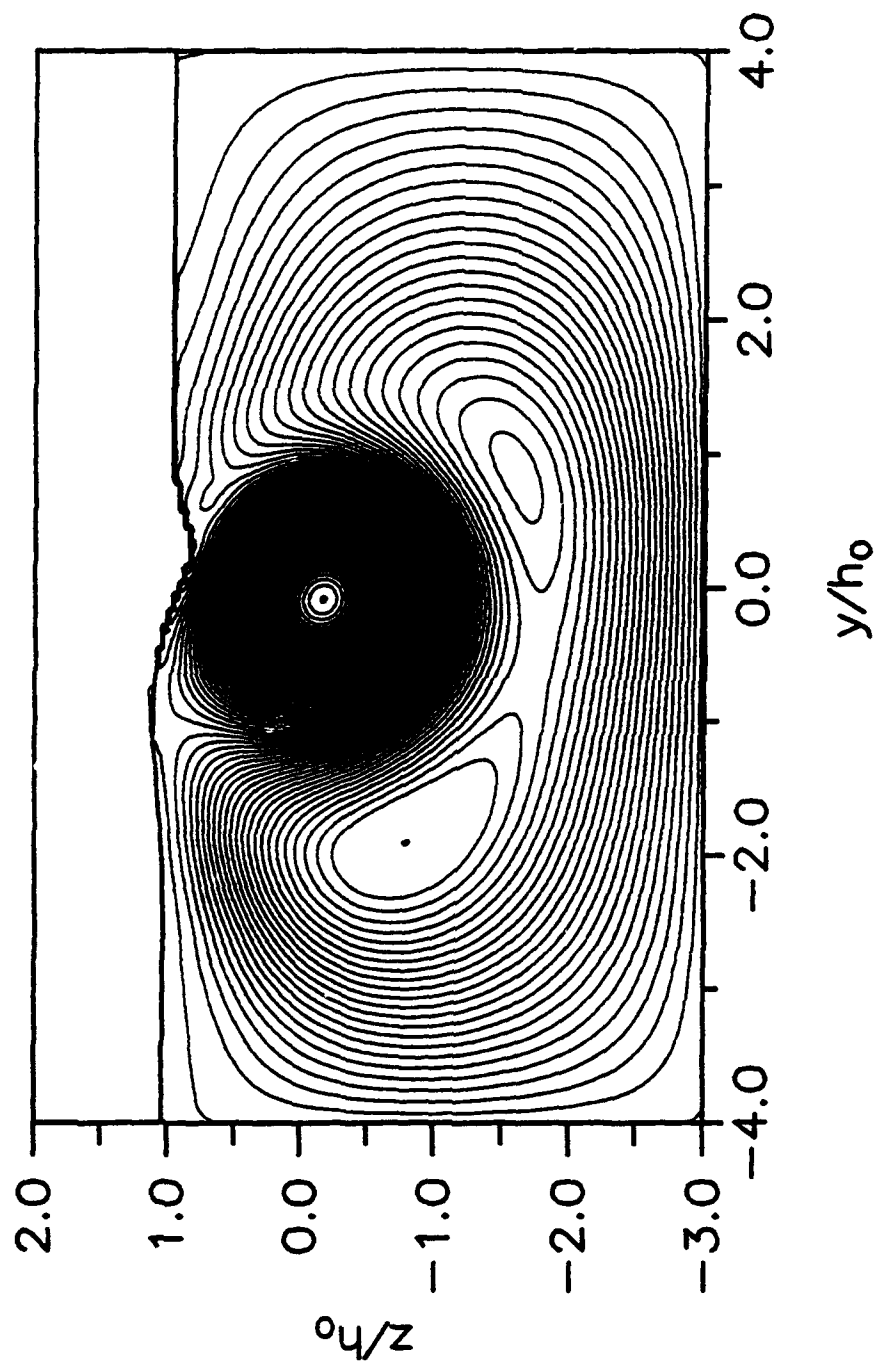Figure 46. Streamlines at T = 29 (Fr = 7.50, Re = 40 and We = 0.033)

72

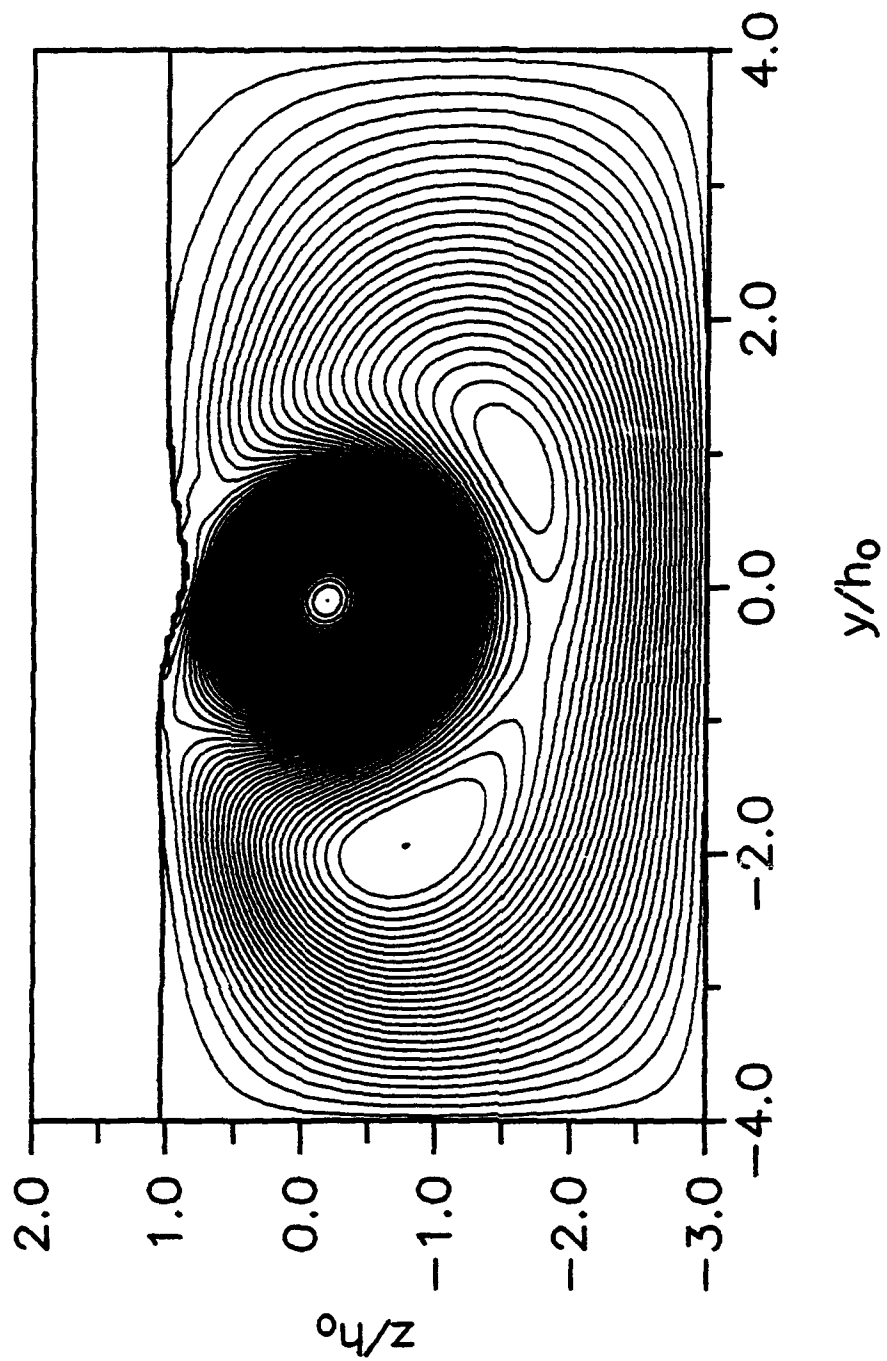Figure 47. Streamlines at T = 30 (Fr = 7.50, Re = 40 and We = 0.033)

REFERENCES

Brackbill, J. U., Kothe, D. B., and Zemach, C., 1992, "A Continuum Method for Modeling Surface Tension," *Journal of Computational Physics*, Vol 100, pp. 335-354.

Kothe, D. B., Mjolsness, R. C., and Torrey, M. D., 1991, "RIPPLE: A Computer Program for Incompressible Flows with Free Surface," Los Alamos National Lab., LA-12007-MS, Los Alamos, NM.

Neubert, D. E., Jr, 1992, *Trailing Vortex/Free-Surface Interaction*, MS Degree Thesis, Naval Postgraduate School, Monterey, CA.

Ohring, S., and Lugt, H. J., 1991, "Interaction of a Viscous Vortex Pair with a Free Surface, " *Journal of Fluid Mechanics*, Vol. 227, pp. 47-70.

Sarpkaya, T. and Henderson, D. O., Jr., 1984, *Surface Disturbances Due to Trailing Vortices*, Technical Report No. NPS-69-84-004, Naval Postgraduate School, Monterey, CA.

Sarpkaya, T., and Suthon, P. B. R., 1991, "Interaction of a vortex couple with a free surface," *Experiments in Fluids*, Vol. 11, pp. 205-207.

Tyvand, P. A., 1991, "Motion of a Vortex Near a Free Surface," *Journal of Fluid Mechanics*, Vol. 225, pp. 673-686.

INITIAL DISTRIBUTION LIST

1. Defense Technical Information Center   2
   Cameron Station
   Alexandria, VA 22304-6145

2. Librarian, Code 52   2
   Naval Postgraduate School
   411 Dyer Rd.,   Rm. 104
   Monterey, CA 93943-5101

3. Department Chairman   1
   Mechanical Engineering Department, Code ME
   Naval Postgraduate School
   699 Dyer Rd,   Rm. M3
   Monterey, CA 93943-5108

4. Professor T. Sarpkaya   5
   Mechanical Engineering Department, Code ME-SL
   Naval Postgraduate School
   699 Dyer Rd,   Rm. M2
   Monterey, CA 93943-5108

5. Naval Engineering Curricular Office   1
   Code 34
   Naval Postgraduate School
   699 Dyer Rd,   Rm. 220
   Monterey, CA 93943-5109

6. Dr. Doug Kothe   1
   Fluid Dynamics Group T-3, MS-B216
   Los Alamos National Lab
   Los Alamos, NM 87545

7. LT Craig F. Merrill, USN   2
   c/o J. F. Matthews
   109 Laurel Ridge Rd.
   Canton, NC 28716